

Phase-Locking of Neurons in the Hippocampus and the Medial Prefrontal
Cortex of the Rat to the Hippocampal Theta Rhythm

by

Evgueniy V. Lubenov

A.B. Psychology and Biology
Harvard University, 1998


SUBMITTED TO THE DEPARTMENT OF BRAIN AND COGNITIVE SCIENCES
IN PARTIAL FULFILLMENT OF THE REQUIREMENTS FOR THE DEGREE OF

DOCTOR OF PHILOSOPHY IN NEUROSCIENCE
AT THE
MASSACHUSETTS INSTITUTE OF TECHNOLOGY

FEBRUARY 2005


© 2005 Massachusetts Institute of Technology. All rights reserved.

Signature of Author:



Department of Brain and Cognitive Sciences
February 2, 2005

Certified by:

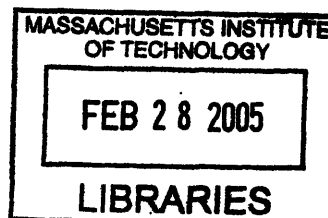


Matthew A. Wilson
Professor of Neurobiology
Thesis Supervisor

Accepted by:



Earl K. Miller
Picower Professor of Neuroscience
Chairman, Department Graduate Committee



ARCHIVES

BYINORIA

Phase-Locking of Neurons in the Hippocampus and the Medial Prefrontal
Cortex of the Rat to the Hippocampal Theta Rhythm

by

Evgueniy V. Lubenov

Submitted to the Department of Brain and Cognitive Sciences
on February 2, 2005 in Partial Fulfillment of the
Requirements for the Degree of Doctor of Philosophy in
Neuroscience

Abstract

The interactions between cortical and hippocampal circuits are critical for memory formation, yet their basic organization at the neuronal network level is not well understood. Here we investigate the timing relationships between neuronal activity in the medial prefrontal cortex of freely behaving rats and the hippocampal theta rhythm. We demonstrate that a significant portion of prefrontal neurons are phase-locked to the hippocampal theta rhythm and we compare the phase-locking properties of prefrontal and hippocampal cells. We also show that prefrontal neurons phase-lock best to theta oscillations delayed by approximately 50 ms and confirm this hippocampo-prefrontal directionality and timing at the level of correlations between single cells. Finally we demonstrate that phase-locking of prefrontal cells is predicted by the presence of significant correlations with hippocampal cells at positive delays up to 150 ms, suggesting that direct hippocampal input has an important contribution to the observed prefrontal phase-locking. The theta entrained activity across cortico-hippocampal circuits described here may be important for gating information flow and guiding the plastic changes that are believed to underlie the storage of information across these networks.

Thesis Supervisor: Matthew A. Wilson
Title: Professor of Neurobiology

*To my parents,
with love and gratitude.*

Contents

1	Introduction	11
1.1	Hippocampal role in memory formation	12
1.2	Role of neocortex in memory formation	12
1.3	Consolidation and cortico-hippocampal interactions	13
1.4	Hippocampo-prefrontal interactions and memory	13
1.5	Hippocampal theta oscillations	14
1.6	Hippocampal neuronal activity and theta oscillations	15
1.7	Theta modulated neuronal activity outside the hippocampus	16
2	Results	19
2.1	Spectral analysis reveals interactions in the theta band	20
2.2	Individual neurons phase-lock to hippocampal theta oscillations	20
2.3	Significant fraction of prefrontal neurons are phase-locked	22
2.4	Phase-locking depends on the micro-structure of the theta rhythm	23
2.5	Maximal prefrontal phase-locking occurs for delayed hippocampal theta oscillations	26
2.6	Covariance between prefrontal and hippocampal cells shows directionality in hippocampo-prefrontal interactions	29
2.7	Covariance between prefrontal and hippocampal cells predicts prefrontal phase-locking	29
3	Discussion	35
3.1	Theta phase-locking and prefrontal theta oscillations	35
3.2	Phase-locking as an independent dimension of neuronal activity	36
3.3	Mechanism responsible for prefrontal phase-locking	36
3.4	Functional significance of prefrontal phase-locking	38
4	Methods	41
4.1	Behavioral tasks	41
4.2	Electrophysiological recordings	41
4.3	Signal source separation	41
4.4	Phase-locking analysis outline	43
4.5	LFP filtering	45
4.6	Instantaneous amplitude/phase decomposition	46
4.7	Effects of theta waveform asymmetry	47
4.8	Phase value distributions φ_U and φ_S	48
4.9	Comparing φ_S and φ_U	48

4.10 Phase-locking detection and characterization	49
4.11 Cross-covariance analysis	50

List of Figures

1	Example of data from chronic multisite tetrode recordings . .	19
2	Spectral analysis reveals hippocampo-prefrontal interactions in the theta band	21
3	Example of theta phase-locking	23
4	Theta phase-locking of hippocampal and prefrontal neurons .	24
5	Phase-locking parameter distributions	25
6	Timing relationship between phase-locked neurons and the theta rhythm	27
7	Cross-covariance between prefrontal and hippocampal cells .	30
8	Cross-covariance between prefrontal and hippocampal cells predicts prefrontal phase-locking	33
9	Example of intermittent theta in a prefrontal LFP	36
10	Firing rhythmicity is independent of phase-locking	37
11	Modular precision machined microdrive array	42
12	Principle of tetrode recordings	43
13	Raw tetrode recordings from the pyramidal cell layer in the CA1 region of the hippocampus	44
14	Phase-locking analysis outline	45
15	Theta phase value distributions of a hippocampal LFP under different phase extraction methods	48

1 Introduction

Many lines of evidence have demonstrated the critical importance of the hippocampus in the formation of new memories [1]. This hippocampal involvement is temporary as memories are gradually established in extra-hippocampal networks through the process of memory consolidation. The predominant conjecture is that during this process hippocampal activity drives the progressive integration of new information in distributed neocortical circuits. While the precise locus and organization of cortical memories and the neuronal mechanisms underlying their establishment remain unknown, previous studies have proposed that the prefrontal cortex plays a key role in this process [2]. Sections 1.1 and 1.2 below examine the evidence for hippocampal and cortical involvement in memory and section 1.3 reviews cortico-hippocampal interactions in light of memory consolidation. Section 1.4 is devoted specifically to discussing the evidence for hippocampo-prefrontal interactions and their functional significance.

If interplay between the hippocampus and the medial prefrontal cortex (mPFC) is indeed central to the process of memory formation, how are the interactions between these two structures organized? To make progress in characterizing these interactions we recorded the simultaneous activity of multiple single neurons in the hippocampus and medial prefrontal cortex of freely behaving rats using chronic multi-tetrode arrays. We focused on characterizing the timing relationships between neuronal activity in the medial prefrontal cortex and the hippocampal theta rhythm. The theta (θ) rhythm is a local field potential (LFP) oscillation in the 4-10 Hz frequency range that has long been recognized as the defining electrophysiological signature of hippocampal activity during active exploratory behavior and REM sleep [3, 4, 5]. Section 1.5 is dedicated to reviewing what is known about hippocampal theta oscillations. The presence of phase-locking of hippocampal neurons to theta oscillations is well established and the evidence is reviewed in section 1.6. Section 1.7 examines the evidence for a global role of theta oscillations and their ability to modulate neural activity outside the hippocampus.

Here we present three new results. First, we demonstrate that the activity of a significant portion of prefrontal neurons is modulated by the hippocampal theta rhythm. Second, we present evidence for directionality in the hippocampo-prefrontal interactions, with hippocampal activity leading the activity in mPFC by approximately 50 ms. Third, we show that direct hippocampal input to mPFC likely contributes significantly to the observed prefrontal phase-locking.

1.1 Hippocampal role in memory formation

The critical involvement of the hippocampus in the formation of memories was established in 1953 after patient H.M. underwent bilateral resection of his medial temporal lobe (MTL) as experimental surgery for the relief of intractable epilepsy [6]. Following the surgery H.M. displayed a profound deficit in his ability to acquire new memories (*anterograde amnesia*) and a temporally graded impairment in recalling old memories (*retrograde amnesia*), yet his other cognitive capacities remained essentially intact [7, 8]. The importance of patient H.M. to current thinking about the process of memory storage can be illustrated by noting that nearly 100 investigators have studied him since 1953 and over 1,750 publications have referenced the original report of his remarkable deficit [9].

The fact that H.M. and clinical cases with similarly localized lesions [10] display selective memory impairments that do not affect other cognitive capacities has led to the notion of *memory systems*: the idea that the process of memory formation involves specialized brain structures, in a manner that parallels the specializations associated with the visual, auditory, sensory, and motor systems [11]. The existence of a multitude of memory systems has been postulated because the conscious and unconscious acquisition of novel information rely on distinct neural substrates [12]. The body of clinical work in humans and lesion studies in nonhuman primates indicate that the hippocampal formation and adjacent cortical areas are an essential part of the medial temporal lobe (MTL) memory system that supports *declarative memory*, i.e. the conscious storage and recall of episodic events and semantic information [13, 12].

1.2 Role of neocortex in memory formation

Despite H.M.'s temporally graded retrograde amnesia (more severely disrupting memories from the more recent past than memories from the more distant past) many of his memories predating the surgery are not affected by the MTL lesion. Therefore memories appear to be ultimately stored outside the hippocampal formation and associated entorhinal, perirhinal, and parahippocampal cortices and most likely reside in neocortical regions [13]. The dominant hypothesis posits that as a new memory is acquired an initial trace forms within the hippocampal system that is needed for recall, but subsequently memories undergo a *consolidation* process, whereby they are progressively integrated within neocortical regions until they can be recalled independently of the hippocampal formation [14, 13, 15].

Direct experimental evidence that neocortex stores memories has been difficult to obtain [16]. Lesions restricted to any particular portion of neocortex affect, but do not eliminate memories completely [17], lending experimental support to the theoretically entertained notion that memories are distributed [14]. If this is indeed the case the electrophysiological correlate of a memory trace will be a pattern of neural activity widely distributed across neocortex, dependent on the prior modification of a great number of synaptic connections [18]. There have been some recent attempts to demonstrate such correlates experimentally [19, 20] that have yielded consistent findings over short timescales (minutes).

1.3 Consolidation and cortico-hippocampal interactions

Consolidation of memories in neocortex presumably takes place under the influence of hippocampal activity during “off-line” periods, such as quiet wakefulness and sleep [21]. Reactivation of hippocampal neural activity patterns during sleep that show correlation with activity patterns recorded during previous behavioral episodes has been experimentally observed [22, 23, 24]. These data provide important evidence that the hippocampal formation is indeed capable of re-expressing activity that contains information about the recent past, yet they shed no light on how such reactivation influences the neocortical network.

Simultaneous recordings from the hippocampus and neocortex have shown evidence consistent with the coordinated re-expression of activity patterns across these structures [19]. Additional evidence for cortico-hippocampal interactions during slow-wave sleep comes from the observed co-occurrence of hippocampal ripples and neocortical spindles during SWS [25, 26]. This finding shows ordering of discrete events in the hippocampal and cortical local field potentials (LFPs) that can control the mode of cortico-hippocampal interactions at the neuronal level [25]. Within the hippocampus the generation of sharp wave/ripple events has been hypothesized to play a central role in a two stage model of memory trace formation [27].

1.4 Hippocampo-prefrontal interactions and memory

The existence of strong functional hippocampo-prefrontal interactions in the rat is supported by anatomical and electrophysiological studies that have demonstrated the existence of a monosynaptic pathway from the hippocampus to the medial prefrontal cortex (mPFC) [28, 29, 30, 31, 32, 33] that is endowed with the ability to undergo activity-dependent modifica-

tions [34, 35, 36, 37, 38]. Disruption of the hippocampo-prefrontal pathway has been shown to impair performance on spatial learning tasks [39, 40], with recent experiments also showing reverse temporal gradients in the involvement of hippocampal and prefrontal circuits [41]. Thus hippocampal circuits appear to be strongly engaged in the early stages of learning and show only limited activation as learning progresses, while the reverse gradient has been documented for prefrontal circuits [42, 43, 44, 41]. This is further corroborated by recent experiments showing that lesions to the hippocampus of rats acquiring trace eyeblink conditioning produce a profound deficit early in training, but have little effect in the late stages of training. In contrast, mPFC lesions produce a strong deficit in the late, but not in the early stages of training [45].

1.5 Hippocampal theta oscillations

Probably the most robust and well documented aspect of brain activity is the ubiquitous presence of field potential oscillations within different frequency bands that are differentially affected by behavioral and brain state. Such oscillations can be measured extracranially in the form of electroencephalographic (EEG) signals or obtained from intracranial depth electrodes positioned inside the brain in the form of local field potential (LFP) fluctuations. By the nature of the recording arrangements large areas of the brain contribute to the EEG signals, while the LFP fluctuations carry information primarily about the current source density within the local neuronal circuit. The synchronized emergence of current sources and sinks within the local neuronal population is therefore a necessary condition for a robust LFP event or oscillatory mode. The geometry of the underlying circuit determines the degree of constructive superposition of the elementary current source dipoles hence the above condition is not sufficient. The absence of a robust LFP event thus does not imply that a large portion of the underlying circuit has not been engaged.

Discovered in 1954, the theta (θ) rhythm, also known as rhythmical slow activity (RSA), is a remarkably robust LFP oscillation in the 4-10 Hz frequency range that represents one of the defining electrophysiological signatures of hippocampal activity [3]. The major behavioral correlates of hippocampal theta in the rat have been demonstrated to be periods of exploratory locomotor behavior and REM sleep, yet other conditions triggering this rhythm possibly exist as well [4, 5].

Within hippocampal CA1 theta oscillations have a complex amplitude-phase depth profile indicating that several underlying current sources and

sinks contribute to the overall wave shape. This is further corroborated by the pharmacological dissociation of atropine-sensitive and atropine-insensitive theta types that co-exist in the intact animal. There is an agreement that the atropine-insensitive theta results from synaptic potentials associated with the entorhinal perforant path input terminating on the distal dendrites of CA1 neurons in stratum lacunosum-moleculare. The atropine-sensitive current source appears to be localized to the pyramidal cell layer and the proximal dendrites in stratum radiatum, yet several hypothesis exist as to its nature. One possibility is that it is associated with perisomatic IPSPs generated by pyramidal cells in response to basket interneuron input. Another possibility is that it results from CA3 input arriving via the Schaffer collaterals and terminating in stratum radiatum.

The medial septum/diagonal band of Broca (MS-DBB) is considered to be the principal pacemaker of the theta rhythm since its lesion or inactivation abolishes theta oscillations in the hippocampus [46]. The presence of mutual connections between MS-DBB and the hippocampus means that theta rhythm generation occurs under closed loop conditions. Resonant properties both at the level of individual pyramidal neurons and at the level of the recurrent CA3 network have been postulated to play an important role in shaping the theta rhythm. Such resonant properties are subject to modification by neuromodulators and thus a permissive role has been assigned to cholinergic and other agents as well.

Theta has been assigned a functional role in spatial and working memory because lesions to the MS-DBB and other manipulations that affect hippocampal theta oscillations produce marked deficits on tasks that rely on these cognitive capacities [46, 47, 48]. Another line of evidence establishes a link between theta rhythmicity and long-term potentiation (LTP), the hypothesized cellular mechanism of memory formation. In particular LTP has been shown to be preferentially induced at theta frequencies [49] and to depend on the instantaneous phase of the hippocampal theta oscillation [50]. Theta also appears to play a role in timing and in global synchronization. On the one hand sensory stimulation is capable of resetting the phase of the hippocampal theta rhythm [51, 52] and on the other both heart rate [53] and ponto-geniculo-occipital (PGO) waves [54] are phase-locked to theta.

1.6 Hippocampal neuronal activity and theta oscillations

In 1971 chronic recordings from the freely-moving rat established that absolute spatial location was a major determinant of pyramidal cell firing in the hippocampus [55]. Because of the tendency of hippocampal pyramidal

cells to fire only within restricted regions of space they became known as “place cells” [56] and the cognitive map theory was put forward postulating that the hippocampus is primarily responsible for tracking the individual’s position in the environment and underlies spatial memory [57] rather than being responsible for declarative memory formation. This apparent contradiction with hippocampal theory derived from clinical and primate studies has been partially resolved through experiments showing that the firing of pyramidal neurons in the hippocampus is not exclusively place-specific but reflects other modalities and behavioral dimensions as well [58, 59, 60].

The quantitative study of the relationship between hippocampal unit activity and the hippocampal theta rhythm was initiated in the early 80s [61, 62, 63]. It revealed that both complex spiking cells (putative pyramidal neurons) and theta-type cells (putative interneurons) within the hippocampus have a tendency to discharge at particular phases of the theta oscillation, thus displaying theta phase-locking. Within CA1 the preferred phase of pyramidal cell firing coincides with the falling edge of the local theta while there exists some disagreement as to whether the preferred phase of interneurons coincides with the troughs or is closer to the peaks of the local theta [63].

The early analysis of phase-locking emphasized the stationary aspects of the interactions between neuronal firing and the theta rhythm. A study of the temporal dynamics of phase-locking over timescales in the order of several theta cycles revealed the phenomenon of theta phase precession, consisting in the gradual advancement of phase values of spikes associated with the traversal of a place field in a linear environment [64]. The resulting correlation between phase values and location within the place field attracted an enormous theoretical interest as it provides an example of an independent dimension different than mean firing rate along which information can be potentially encoded [65, 66].

1.7 Theta modulated neuronal activity outside the hippocampus

Theta related activity is present in many subcortical structures projecting to the hippocampus and within the limbic system. Cholinergic and GABAergic neurons within the medial septum drive the hippocampal theta rhythm and are consequently phase-locked to it [67]. Similarly subgroups of neurons within the hypothalamic nuclei projecting to the hippocampus, i.e. the posterior hypothalamic nucleus, the supramammillary nucleus, and the nuclei of the mammillary body, are coupled to theta oscillations at different pre-

ferred phases [68]. The dorsal raphe [69] and the ventral tegmental nucleus of Gudden [70] should also be added to the list of subcortical systems showing theta related activity. In addition to the hippocampal formation, unit activity in other limbic system structures including the entorhinal cortex [71] and the amygdala [72] show modulation by the theta rhythm.

Apart from structures closely linked to the hippocampus, theta modulated activity has been recorded from the inferior colliculus [73] and the auditory cortex [74] suggesting that theta rhythmicity may play a role in auditory information processing. Similar observations have been made in the lateral geniculate nucleus [75] and the superior colliculus [76] indicating a role in visual processing. Some neurons within the posterior cingulate cortex are also theta phase-locked [77]. These studies suggest that hippocampal theta oscillations provide access to rhythm generators that might play a global synchronization role.

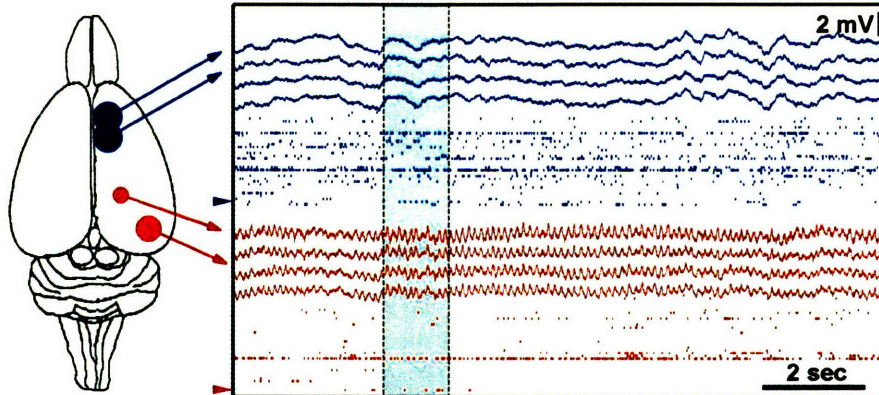


Figure 1: **Example of data from chronic multisite tetrode recordings:** Four simultaneously recorded prefrontal local field potential (LFP) traces (in blue) and four hippocampal LFP traces (in red), together with rasters of single-unit activity in the prefrontal cortex (35 neurons) and hippocampus (37 neurons). The total duration of the LFP traces shown here is 13 seconds. The brain diagram on the left indicates the recording sites of the hippocampal (red) and prefrontal (blue) recordings. For all figures hippocampal and prefrontal examples are shown in red and blue respectively.

2 Results

We recorded simultaneously local field potential (LFP) traces and single unit activity in the hippocampus and the medial prefrontal cortex of rats performing a variety of spatial navigation tasks (fig. 1). Here we report, to our knowledge for the first time, that neurons in the medial prefrontal cortex are phase-locked to the hippocampal theta rhythm. We quantitatively characterize and compare the basic phase-locking properties of prefrontal and hippocampal cells and demonstrate that the observed phase-locking is not simply due to intrinsic rhythmicity of neuronal firing in the θ frequency band, but explicitly depends on the entrainment of spiking activity to the ongoing frequency fluctuations of the hippocampal theta rhythm.

Furthermore, we show that while hippocampal neurons phase-lock best to simultaneously occurring theta oscillations, prefrontal cells phase-lock best to theta oscillations delayed by approximately 50 ms. This result is consistent with a directionality in the hippocampo-prefrontal interactions with hippocampal activity leading the activity in prefrontal cortex. We further demonstrate this directionality at the level of single cell interactions.

We also show that the phase-locking of a prefrontal cell is predicted by the presence of significant correlations with a subset of hippocampal cells over a range of positive delays up to 150 ms, suggesting that direct hippocampal input has a considerable contribution to the observed prefrontal theta phase-locking.

2.1 Spectral analysis reveals interactions in the theta band

As a first step in the exploration of the relationship between prefrontal and hippocampal activity we applied classical spectral analysis to the hippocampal and prefrontal LFPs, as well as hybrid spectral analysis to spike train and LFP data. The spectral characterization of the data offers descriptive statistics that can reveal linear interactions between signals over the entire frequency range up to the Nyquist limit. Thus the frequency bands in which interactions are present can be identified for further study.

The power spectral density (PSD) estimate of the hippocampal LFP displayed a prominent theta peak between 7 and 8 Hz, as expected (fig. 2a), while no equivalent peak was present in the prefrontal PSD estimate (fig. 2c). The spectra of most hippocampal neurons and a fraction of prefrontal cells also displayed significant peaks in the θ band, indicating theta rhythmicity in their firing (fig. 2b). The spectrograms of the hippocampal and cortical LFPs indicated that spectral content was relatively stable over the time course of the recording sessions. While the hippocampal and prefrontal LFPs were strongly coherent in the δ (0-4 Hz) band, they were only marginally coherent in the θ band (fig. 2h). Overall, the activity of individual neurons did not show significant interactions with prefrontal LFPs (fig. 2i). This was in striking contrast to the significant theta band coherence that a subset of hippocampal and *prefrontal* neurons displayed with respect to the hippocampal LFPs (fig. 2g).

2.2 Individual neurons phase-lock to hippocampal theta oscillations

The coherence estimate at a given frequency ω relies on computing the complex correlation coefficient between the Fourier components at ω of the two input signals (fig. 2). Thus the pattern of both amplitude and phase variation contribute to the magnitude of the coherence and their influences cannot be separated. To directly characterize the timing relationship of neuronal firing to the hippocampal theta rhythm, the hippocampal LFP was first band-pass filtered in the θ band (4-10 Hz) and the filtered trace was de-

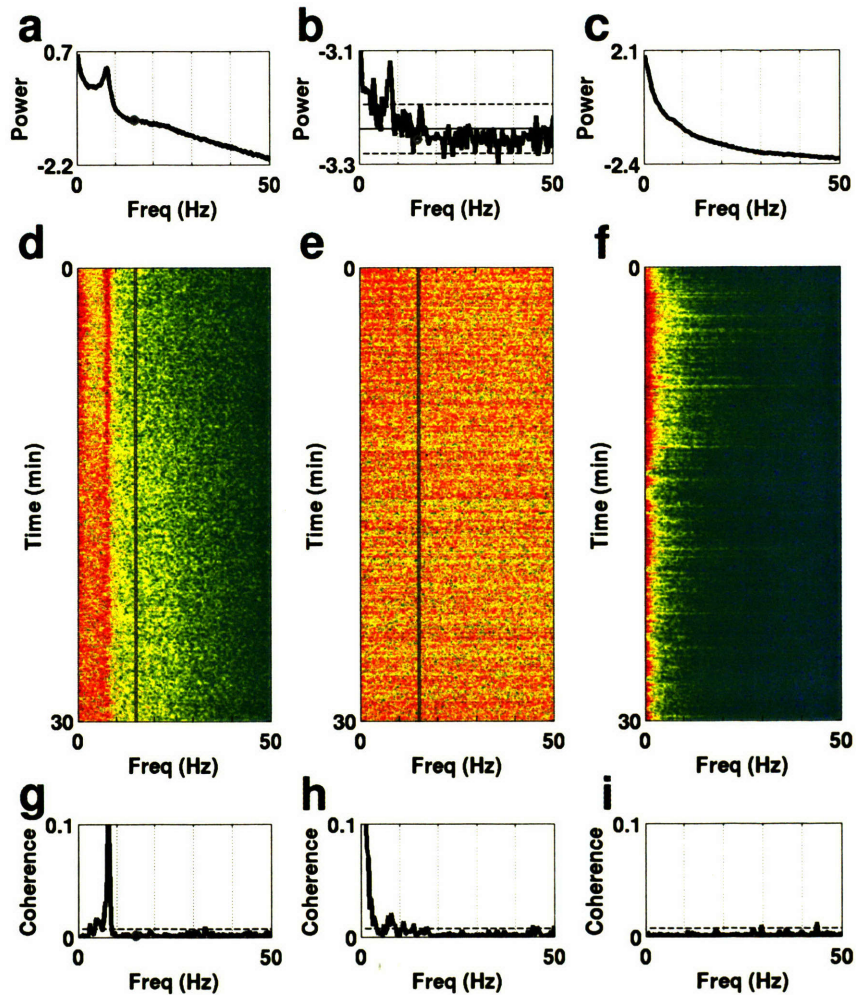


Figure 2: **Spectral analysis reveals the presence of hippocampo-prefrontal interactions in the theta band:** Power spectral density (PSD) estimates of simultaneously recorded hippocampal LFP (a), spike train of a prefrontal cell (b), and prefrontal LFP (c). Note the elevated power in the theta (θ) band (4-10 Hz) in (a) and (b), in contrast to (c). Corresponding spectrograms (d), (e), (f) over 30 minutes of recording. Note the consistent presence of θ power in the hippocampal LFP (d) and the noisy nature of the spike train spectral estimate (b) and (e). (to be cont.)

Figure 2: **(cont.)** The hybrid coherence estimate between the hippocampal LFP and the spike train (**g**) indicated significant interaction (values above dotted line) in the θ band. In contrast, the coherence between the cortical LFP and the spike train (**i**) was not significant. The coherence between the two LFPs (**h**) was very significant in the δ (0-4 Hz) band and only marginally significant in the θ (4-10 Hz) band. The coherence value at a given frequency (dot in **g**) gives the absolute value of the correlation between the corresponding Fourier components over time (lines in **d**) and **e**).

composed into instantaneous amplitude, $\rho(t)$, and phase, $\phi(t)$, components. A spike occurring at time τ was assigned phase value $\phi(\tau)$. In this fashion, the spike train of each cell was converted into a sequence of unit length vectors oriented by the phase values of their corresponding spikes (fig. 3). The *mean resultant vector* was computed as the average of the vector sequence and the *mean direction* or *mean preferred phase* as the orientation of the mean resultant vector (methods section). Intuitively, if the firing of a given neuron is independent of the theta rhythm, the distribution of its phase values φ_S will be random, i.e. uniform on $[-\pi, +\pi)$, and its mean resultant vector will be short. Conversely, if the firing of a given neuron is phase-locked to the theta rhythm, its phase value distributions will be unimodal and its resultant vector will be long. The significance of phase-locking can thus be evaluated using Rayleigh's Z statistic, which is directly related to the length of the mean resultant vector (methods section).

2.3 Significant fraction of prefrontal neurons are phase-locked

Approximately 80 % of hippocampal cells and 40 % of prefrontal cells that we recorded were significantly phase-locked to the hippocampal theta rhythm (fig. 4). The proportions of phase-locked cells varied very little with respect to the phase extraction method (typical standard error of the mean less than 1%). Since the presence of phase-locking only indicates departure from uniformity in the phase value distribution of a given cell, we further characterized the locking properties of individual units by fitting von Mises densities to their corresponding phase value distributions (fig. 4a-d).

The von Mises distribution is the circular analog of the normal distribution and is parametrized by a mean direction or preferred phase μ and concentration parameter κ , with larger κ values corresponding to more peaked distributions (methods). As has been previously reported, most hippocampal neurons had preferred phases on the falling edge of the theta cycle (fig. 5a) resulting in a unimodal μ distribution [63, 5]. In contrast, the prefrontal distribution of preferred phases relative to the hippocampal theta

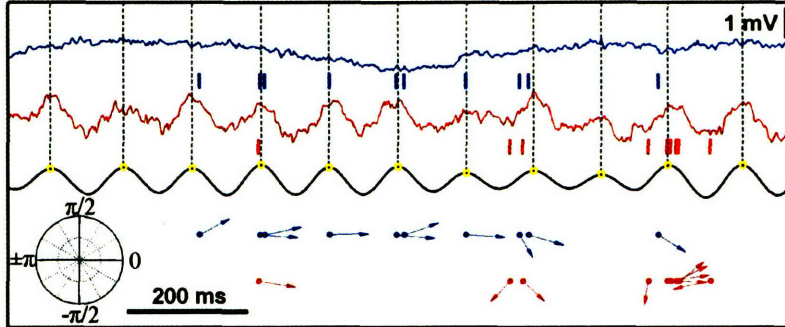


Figure 3: **Example of theta phase-locking:** The gray region in fig. 1 expanded. A prefrontal LFP trace and the spike train of a prefrontal neuron are shown in blue. Underneath in red is a hippocampal LFP trace and the activity of a place cell as the animal traverses its place field. The two selected neurons are marked by arrows in fig. 1. Shown in black is the hippocampal trace band-pass filtered in the theta range (4-10 Hz). The yellow dots and the gray dotted lines indicate the position of the peaks of the theta rhythm which were automatically identified as described in the methods. The phase-locking of the hippocampal pyramidal cell is evident. Moreover note that despite the lack of any apparent theta rhythmicity in the prefrontal LFP trace there is still a striking phase-locking of the prefrontal neuron to the hippocampal theta oscillation which is recorded at a significant distance away from the prefrontal neuron ($\sim 7\text{mm}$). The unit vector sequences corresponding to the cortical (blue) and hippocampal (red) spike trains are shown at the bottom. Each unit vector is oriented by the phase value of its corresponding spike (peaks correspond to 0 radians, and troughs to $\pm\pi$).

oscillations was wider, and centered close to the peak of the theta cycle. It should be noted that the theta rhythm was always extracted from a particular tetrode in each animal and it was therefore nonlocal to the majority of the recorded cells. Neurons in both areas displayed a broad range of degrees of phase-locking and corresponding κ values, with the hippocampal population exhibiting a tendency toward more concentrated phase value distributions compared to the prefrontal one (fig. 5b).

2.4 Phase-locking depends on the micro-structure of the theta rhythm

Since the theta rhythm is an oscillatory process constrained to a narrow frequency band (4-10 Hz), it is important to show that the phase-locking

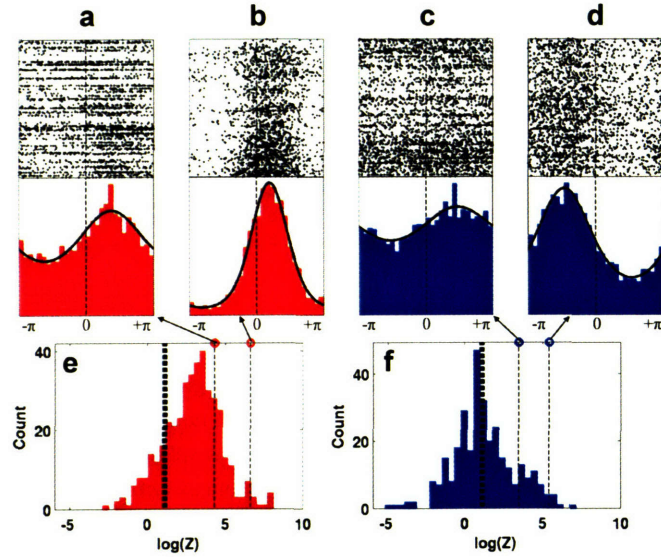


Figure 4: **Theta phase-locking of hippocampal and prefrontal neurons: (a-d)** Examples of phase-locking to the hippocampal θ rhythm for two hippocampal (a,b) and two prefrontal cortical units (c,d). The spike trains of individual units were broken up at the troughs of the hippocampal theta rhythm and the resulting segments were stacked up to form the theta-triggered rasters shown on top. Below are the corresponding phase value distributions. Also shown are the von Mises fits for each example parameterized by mean direction μ and concentration parameter κ . Parameter pairs (μ, κ) are (a) (1.18, 0.33), (b) (0.60, 1.42), (c) (1.50, 0.19), (d) (-1.47, 0.61). (e,f) Distribution of log transformed Rayleigh's Z , the statistic used to evaluate the significance of phase-locking for hippocampal (e) and prefrontal (f) units. Significance probability associated with Z (based on 50 spikes or more) is $p = e^{-Z}$ and therefore $\log(Z) = \log(-\log(p))$. Thick black lines indicate the $p = 0.05$ significance threshold, thus all values of $\log(Z)$ to the right of these lines are significant at that confidence level. Note that log is applied to tighten the Z distribution, yielding a double log scale, so that $\log(Z)$ values [1, 2, 3, 4, 5] approximately correspond to p values [$10^{-1}, 10^{-3}, 10^{-9}, 10^{-24}, 10^{-64}$]. $80.85\% \pm 0.63\%$ (332 ± 2.6 out of 411) of hippocampal and $44.03\% \pm 0.50\%$ (139 ± 1.6 out of 316) of prefrontal units were phase-locked to the hippocampal theta rhythm ($p = 0.05$). When analysis is restricted to unique single units the corresponding figures are $81.34\% \pm 1.84\%$ (90 ± 2 out of 111) and $34.77\% \pm 0.63\%$ ($39 \pm .7$ out of 113) for the hippocampus and prefrontal cortex respectively. The displayed distributions are based on phase extraction using the Hilbert method while the means and their associated standard errors result from averaging over values based on 7 complementary phase extraction methods (see methods).

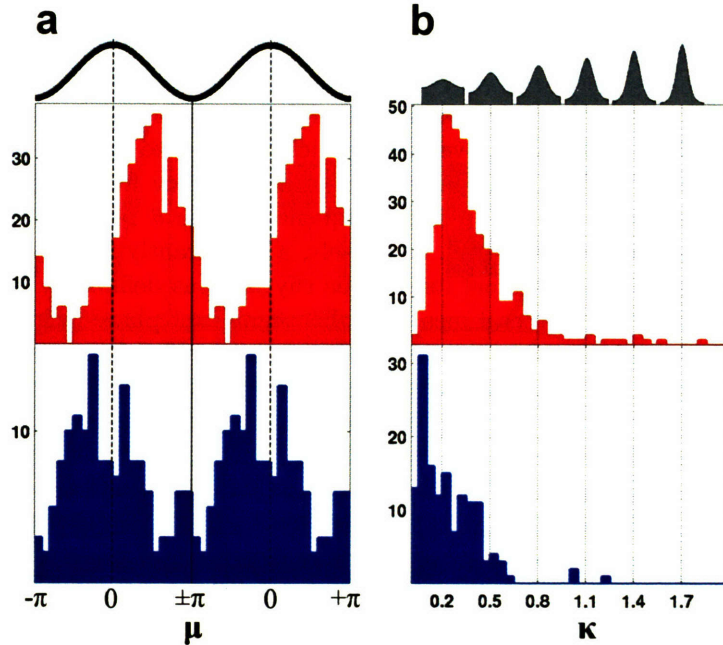


Figure 5: Phase-locking parameter distributions: (a) Histograms of mean preferred phase μ for all significantly phase-locked hippocampal (top) and prefrontal (bottom) units replicated over two θ cycles for visual clarity. Most hippocampal units have preferred phases on the falling edge of the θ cycle ($\bar{\mu} = 1.54$, circular variance 0.54), while the prefrontal population displays a wider distribution centered around the peak ($\bar{\mu} = -0.60$, circular variance 0.72). The distributions offer only qualitative description since units from different animals were referenced against LFP signals not necessarily derived from precisely the same depth in the hippocampus, therefore introducing a potential phase offset that likely shifts and broadens the overall distribution of preferred phases. (b) Histograms of phase value distribution concentration parameters κ for significantly phase-locked hippocampal (top) and prefrontal (bottom) units. The gray von Mises distributions shown on top visually indicate the degree of modulation corresponding to six labeled concentration parameter values. The hippocampal population is biased toward more concentrated phase value distributions ($\bar{\kappa} = 0.39$, $\sigma_{\kappa} = 0.26$) than the prefrontal population ($\bar{\kappa} = 0.24$, $\sigma_{\kappa} = 0.20$). The phase value distributions of 85 % of the prefrontal units and 61 % of the hippocampal units were fit well by the von Mises density (U^2 goodness of fit test, $p=0.05$). In most remaining cases the fit was imperfect due to subtle deviations in the phase value distribution such as the presence of slight asymmetry, rather than due to drastic model departures such as multimodality. Altogether κ captured well the degree of modulation in the phase value distributions.

properties described above do not arise simply from intrinsic rhythmicity in the firing of hippocampal and prefrontal neurons in the same frequency range. Theta oscillations are not constant in frequency but show a pattern of small frequency fluctuations over time which we refer to as the *micro-structure* of the theta rhythm. Because of such frequency fluctuations, a neuron with rhythmic firing at a fixed frequency in the θ range will not necessarily show phase-locking and, conversely, a significantly phase-locked neuron will not necessarily reveal itself to be rhythmic as defined by auto-correlation or interspike interval measures. For significant phase-locking to be present the spike train of a given neuron must match the micro-structure of the theta rhythm. This implies that perturbing the temporal alignment between the theta rhythm and a spike train should decrease the degree of phase-locking in proportion to the size of the perturbation. We confirmed this explicitly by showing that the degree of phase-locking computed at different temporal offsets between the theta rhythm and neuronal spike trains decays with increasing offsets (fig. 6). Temporal offsets of 1 second or more abolish the statistical significance of phase-locking, rendering the phase value distributions close to uniform for both hippocampal (fig. 6a) and prefrontal (fig. 6b) neurons. Note that introducing a temporal offset between the theta rhythm and a given spike train affects only the joint statistics of these two processes without affecting the statistics of the processes themselves. This analysis establishes that the observed phase-locking is not simply due to intrinsic rhythmicity of neuronal firing in the θ frequency band, but explicitly depends on the entrainment of spiking activity to the ongoing frequency fluctuations of the hippocampal theta rhythm.

2.5 Maximal prefrontal phase-locking occurs for delayed hippocampal theta oscillations

A striking aspect of figure 6 is that maximal phase-locking need not occur when the spike train and the LFP trace are aligned, i.e. at time offset $\tau = 0$. For example, the hippocampal cell (fig. 6a) is maximally locked to the hippocampal theta rhythm shifted back in time ($\tau_{max} = -45.89$ ms), while the prefrontal cell is maximally locked to the theta rhythm shifted forward in time ($\tau_{max} = 78.40$ ms). In other words, the example hippocampal cell is maximally locked to the future of the LFP signal, while the prefrontal cell to its past. This observation is consistent with the interpretation that the current sources and sinks associated with the firing of this hippocampal cell contribute to the LFP signal, while the firing of this prefrontal cell is influenced by theta-modulated hippocampal outputs after some delay.

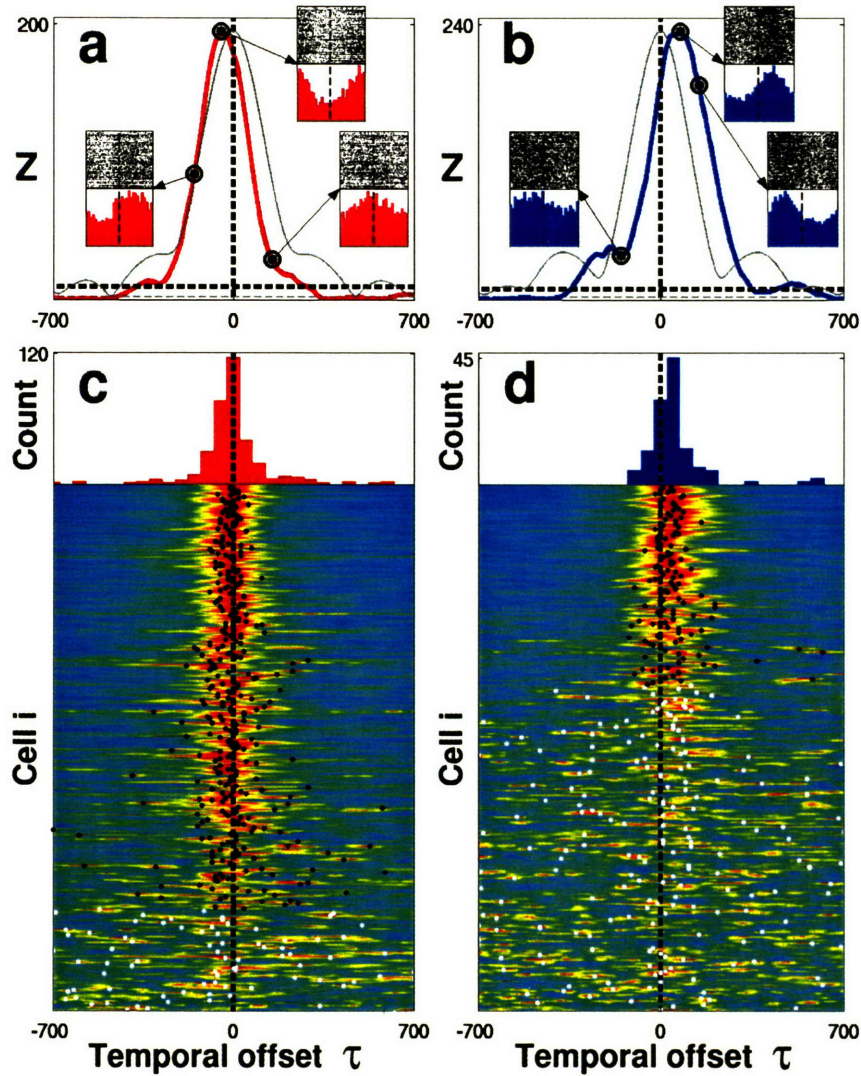


Figure 6: **Timing relationship between phase-locked neurons and the theta rhythm:** (a,b) Rayleigh's Z computed as a function of temporal offset τ between the hippocampal θ trace and the spike train of a hippocampal (a) and a prefrontal cortical (b) neuron ($\tau > 0$ indicates shifting the spike train back in time or equivalently shifting the θ trace forward). Behind in gray are the scaled envelopes of the autocorrelation functions of the filtered hippocampal θ traces used in each example. Note the rapid decay in Z value and autocorrelation with increase in time offset (to be cont.).

Figure 6: (cont.) The inserts show explicitly the θ -triggered rasters and phase value distributions at temporal offsets $\tau = -150, -45.89, 150$ ms with corresponding (μ, κ) pairs $(1.29, 0.36), (2.96, 0.53), (-0.13, 0.20)$ for (a) and $\tau = -150, 78.40, 150$ ms with $(-1.13, 0.17), (1.18, 0.42), (-1.69, 0.37)$ for (b). Z decays at a similar rate as the reference θ traces decorrelate and sufficiently large time offsets ($|\tau| > 1$ s) abolish the significance of phase-locking and render the phase value distributions uniform. This demonstrates that the observed phase-locking explicitly depends on the entrainment of neuronal firing to the ongoing frequency fluctuations of the hippocampal theta rhythm. Note that in these examples the hippocampal unit was maximally phase-locked to the future of the LFP signal (i.e. at $\tau = -45.89 < 0$), while the prefrontal unit was maximally phase-locked to the past of the LFP signal (i.e. at $\tau = 78.40 > 0$). (c,d) Pseudocolor panels show analysis as in (a,b) carried out for all hippocampal (c) and prefrontal (d) units. Rayleigh's Z as a function of temporal offset τ for each unit is normalized by its maximal value Z_{max} occurring at τ_{max} , color coded, and displayed in a row. Rows are sorted by Z_{max} in descending order. Black and white dots indicate the location of τ_{max} and the color signifies whether (black) or not (white) Z_{max} exceeded the significance threshold. The significance threshold was adjusted to $p = \frac{0.05}{141}$ since a hypothesis test can be thought to occur at each of the 141 time offset values (τ varied between ± 700 ms in 10 ms increments). 330 out of 411 hippocampal and 120 out of 316 prefrontal units had above threshold Z_{max} . Note that the significance of phase-locking of these units tends to decay at a similar rate as can be witnessed by the uniform thickness of the red band along the midline. Also, note that the red band and τ_{max} occur along the zero offset midline for the hippocampal population (c), but are clearly shifted to a positive offset for the prefrontal population (d). This is explicitly demonstrated in the histograms above showing the distributions of the significant τ_{max} (black dots) for the hippocampal population ($\bar{\tau}_{max} = -3.94 \pm 7.15$ ms) and the prefrontal population ($\bar{\tau}_{max} = 49.92 \pm 10.76$ ms). Hippocampal units were therefore maximally phase-locked to the present of the hippocampal θ rhythm, while the prefrontal units to its past.

At the population level the hippocampal distribution of offsets τ_{max} yielding maximal phase-locking was centered around zero offset ($\bar{\tau}_{max} = -3.94 \pm 7.15$ ms) and exhibited marked variability ($\sigma_{\tau_{max}} = 129.96$ ms) (fig. 6c). In contrast the prefrontal distribution of τ_{max} was centered at a positive offset ($\bar{\tau}_{max} = 49.92 \pm 10.76$ ms) and exhibited similar variability as the hippocampal population ($\sigma_{\tau_{max}} = 117.41$ ms) (fig. 6d). The prefrontal population mean $\bar{\tau}_{max}$ was significantly different from 0 with mean z score of 4.25 averaged over the different phase extraction methods.

One might hypothesize that the time offset associated with maximal locking depends on the preferred phase and/or concentration parameter of

a given cell. We examined this hypothesis explicitly by fitting a circular regression for τ_{max} and μ and a standard linear regression for τ_{max} and κ , but did not detect any significant interaction ($p = 0.05$). Therefore the time offset associated with maximal locking appears to be an independent parameter describing the theta phase-locking properties of a neuron.

2.6 Covariance between prefrontal and hippocampal cells shows directionality in hippocampo-prefrontal interactions

The fact that prefrontal cells phase-lock best to time-delayed theta oscillations (section 2.5, fig. 6d), suggests that prefrontal firing is influenced by theta-modulated hippocampal inputs after a mean delay of approximately 50 ms. To examine this hypothesis more directly at the single cell level we computed the cross-covariance functions between all pairs of simultaneously recorded prefrontal and hippocampal cells. This analysis revealed that a specific subset of prefrontal cells indeed had significant correlations with subsets of the simultaneously recorded hippocampal cells at positive lags up to 150 ms, confirming the directionality and mean lag predicted by the analysis of section 2.5 (fig. 7).

The interactions of each prefrontal cell i with the population of simultaneously recorded hippocampal cells were summarized through the standardized mean cross-covariance $Q_i(u)$ (fig. 7d, 7h, methods). Approximately 10 % of the prefrontal units displayed mean cross-covariance structure similar to the one exemplified in figs. 7d and 7h, i.e. having one very significant 50-100 ms wide peak or trough, occupying a range of positive lags up to 150 ms. The rest of the units did not exhibit any clear cross-covariance structure, but instead had much narrower, less prominent peaks and troughs, distributed over the entire range of positive and negative lags. We confirmed that most of the latter were spurious cross-covariances, an expected artifact arising in connection with low mean firing rates, that disappeared almost completely when the analysis was restricted to cell pairs with sufficient number of spikes (see methods).

2.7 Covariance between prefrontal and hippocampal cells predicts prefrontal phase-locking

To explore the possible contribution of hippocampal inputs to prefrontal theta phase-locking we compared the mean cross-covariances of phase-locked prefrontal units (fig. 8c) and non phase-locked prefrontal units (fig. 8d).

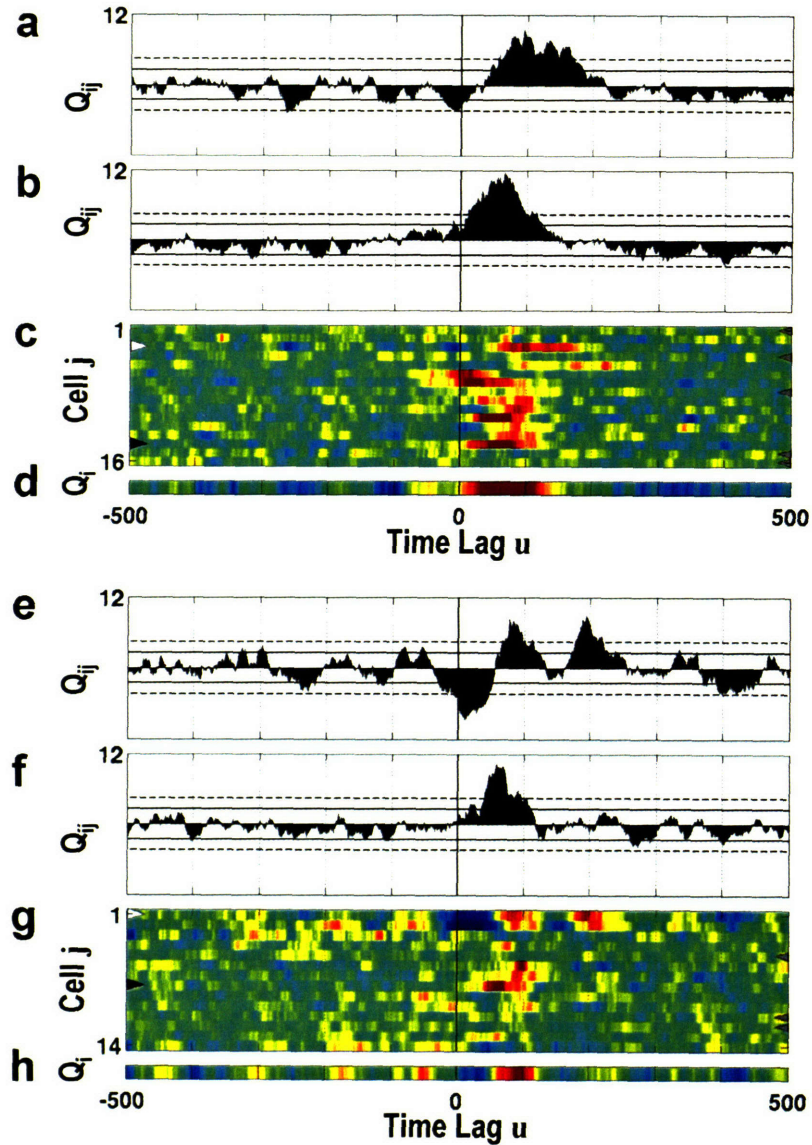


Figure 7: **Cross-covariance between prefrontal and hippocampal cells:** (a,b) Standardized cross-covariance $Q_{ij}(u)$ between prefrontal unit i and two simultaneously recorded hippocampal units (a) $j = 4$, (b) $j = 7$ ($u > 0$ indicates shifting unit i back in time or equivalently shifting unit j forward) (to be cont.).

Figure 7: (cont.) The solid and dashed horizontal lines indicate the 99% and 99.999% confidence limits under the assumption of independence. If $Q_{ij}(u)$ crosses one of the dashed horizontal lines, the hypothesis of independence can be rejected at $\alpha = 0.01$. Note the prominent peaks in (a) and (b), indicating that the given prefrontal unit had a significantly elevated probability of firing between 50 and 150 ms after hippocampal unit 4 and between 0 and 100 ms after hippocampal unit 7. (c) Each row in the pseudocolor plot shows $Q_{ij}(u)$ between the given prefrontal unit i and one of the 16 hippocampal units j that were simultaneously recorded. The colormap, shown in fig. 8, represents significant positive values in red, significant negative values in blue, and non-significant values in green. Examples (a) and (b) are marked by the white and black arrows on the left. Note that the peak in the cross-covariance occurs at different positive lags between 0 and 150 ms for the different hippocampal units, and that there are some hippocampal units that show no significant interaction with the given mPFC unit, i.e. $j = 15$ and $j = 16$. (d) Standardized mean cross-covariance $Q_i(u)$ between the given prefrontal unit and the population of hippocampal units. The pairwise cross-covariances $Q_{ij}(u)$ that are not significantly different from 0, marked with gray arrows on the right of (c), do not enter in the computation of $Q_i(u)$. (e,f,g,h) Plots similar to (a,b,c,d) showing $Q_{ij}(u)$ between another prefrontal unit and all 14 hippocampal units that were simultaneously recorded. Note the more complex, multimodal structure of $Q_{ij}(u)$ and the significant dip around 0 ms in (e). While unit $j = 2$ displays cross-covariance structure similar to that of unit $j = 1$, unit $j = 8$, shown in (f), exhibits a unimodal peak around 50 ms, similar to (b). Finally note that the dip around 0 ms is attenuated in the standardized mean cross-covariance (h), indicating that cancellation of significant cross-covariance structure is possible in $Q_i(u)$.

Essentially all prefrontal units that had a significant cross-covariance peak or trough at positive lags up to 150 ms were phase-locked (fig. 8c), while none of the units that were not phase-locked exhibited an equivalent cross-covariance feature (fig. 8d). This was confirmed further by comparing the average cross-covariance across all phase-locked units, $\langle Q_i(u) \rangle_L$, with the corresponding average taken over all non phase-locked cells, $\langle Q_i(u) \rangle_{\bar{L}}$ (fig. 8e). The average cross-covariance of the phase-locked cells had a prominent peak between 40 and 120 ms and a smaller trough between -125 and -100 ms. Furthermore it was significantly different from the average cross-covariance of the non phase-locked cells in those intervals (fig. 8e). This was consistent with the interpretation that the firing of hippocampal units influenced the firing of phase-locked prefrontal units.

We also confirmed that the apparent absence of prominent features in the cross-covariances of non phase-locked units (fig. 8d) was not due to the

potential negation of significant features of opposite sign that could have occurred in the computation of individual $Q_i(u)$ (fig. 7h). In particular, for each prefrontal cell we computed the mean squared cross-covariance, $Q_i^s(u)$, a non-negative measure of the significance of the interactions as a function of lag and independent of sign. The average $Q_i^s(u)$ across the population of non phase-locked units was indeed essentially flat and significantly different from the corresponding average taken across the phase-locked units, which showed a prominent peak between 20 and 120 ms (fig. 8f).

Thus the presence of significant interactions at positive lags up to 150 ms in the mean cross-covariance of a prefrontal unit with the hippocampal population was a perfect predictor of phase-locking for that prefrontal cell. Such significant cross-covariances were not observed for all phase-locked prefrontal units, which could simply be due to the limited sampling of the hippocampal population. These results suggest that direct hippocampal input contributes significantly to the observed prefrontal theta phase-locking, and may indeed be required.

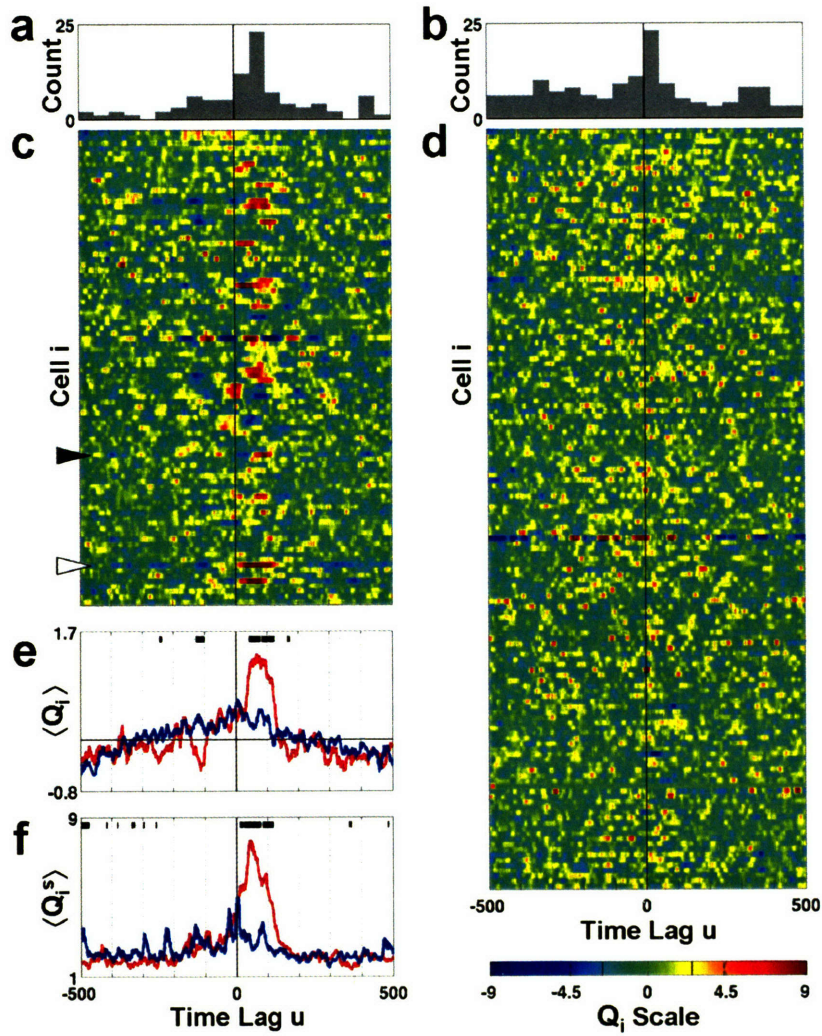


Figure 8: **Cross-covariance between prefrontal and hippocampal cells predicts prefrontal phase-locking:** (a,b,c,d) Each row in the pseudocolor panels (c,d) shows a standardized mean cross covariance, $Q_i(u)$, between a given prefrontal unit i and the population of hippocampal units. All significantly phase-locked prefrontal units are stacked in (c) and all remaining prefrontal units in (d). The examples from fig. 7d and 7h are indicated by the white and black arrows on the left in (c) (to be cont.)

Figure 8: **(cont.)** (a) and (b) show the distribution of time lags, u_i^{\max} , at which each of the $Q_i(u)$ shown in (c) and (d), respectively, achieved their maximal absolute values (50 ms bins). Note that many $Q_i(u)$ of the phase-locked units showed significant peaks at positive time lags up to 150 ms, as can be witnessed by the prominent red patches to the right of the midline in (c). This tendency is also reflected in the peak of the 50-100 ms bin in the distribution of u_i^{\max} shown above. The non phase-locked population showed a tendency for peak absolute values between 0 and 50 ms, as can be seen in (b), but no salient cross-covariance features were discernible in (d). (e) The average $Q_i(u)$ for all significantly phase-locked units $i \in L$, $\langle Q_i(u) \rangle_L$, is shown in red, and the average $Q_i(u)$ for all remaining units $i \in \bar{L}$, $\langle Q_i(u) \rangle_{\bar{L}}$, in blue. Thus the red curve is the average of all rows in (c), while the blue curve is the average of all rows in (d). The black intervals at the top of the figure indicate the corresponding ranges of lags over which $\langle Q_i(u) \rangle_L$ and $\langle Q_i(u) \rangle_{\bar{L}}$ were significantly different ($p = .95$, Behrens-Fisher test). Note the significant peak of $\langle Q_i(u) \rangle_L$ between 40 and 120 ms and the dip between -125 and -100 ms. Both features indicate that the phase-locked mPFC units tended to discharge after the hippocampal units. (f) $\langle Q_i^s(u) \rangle_L$ in red and $\langle Q_i^s(u) \rangle_{\bar{L}}$ in blue (see methods). Note that $\langle Q_i^s(u) \rangle_{\bar{L}}$ is relatively flat and significantly different from $\langle Q_i^s(u) \rangle_L$ between 20 and 120 ms, demonstrating that the absence of structure in (d) is not due to the cancellation of significant features that might have occurred in the computation of the individual $Q_i(u)$. Thus the prefrontal units that were not phase-locked indeed did not display significant cross-covariance structure with the hippocampal units over ± 500 ms time lags.

3 Discussion

3.1 Theta phase-locking and prefrontal theta oscillations

As demonstrated in section 2.2 the firing of a significant fraction of prefrontal neurons was modulated by the hippocampal theta rhythm. This prefrontal theta phase-locking was present even when there was little apparent theta power in the prefrontal LFPs (figs. 1, 2, 3). The current sources and sinks in mPFC arising in connection with phase-locking to the hippocampal theta rhythm may not contribute significantly to the θ band of the macroscopically observed local field potential for several reasons. First, the relevant current generators within mPFC might have a random spatial arrangement, therefore giving rise to “closed fields” [5]. While this is possible for inputs terminating on prefrontal interneurons, it is less likely to be the case for pyramidal cells, given the characteristic parallel organization of their dendrites and afferents. Second, inputs to different phase-locked neurons might arrive over different phases of the theta cycle, eliminating the synchrony required for a prominent LFP oscillatory mode. The fact that the mean preferred phase distribution of phase-locked prefrontal cells was non-uniform argues against this hypothesis (fig. 5). Third, the layer of prefrontal cortex yielding the highest number of single unit data might be close to the null point of the prefrontal theta dipole. If so, the apparent absence of theta power in the prefrontal LFPs could be explained by the bias in the placement of the recording electrodes. Finally, hippocampo-prefrontal feed-forward inhibition rather than excitation might be the major contributor to the observed phase-locking. We discuss how this can explain prefrontal phase-locking even in the absence of θ power in prefrontal LFPs in section 3.3 below.

The presence of clear but short-lived theta oscillations in prefrontal LFPs (fig. 9) argues that the mPFC circuitry can generate macroscopically observable theta oscillations, but that these oscillations have more complex behavioral correlates than the hippocampal theta rhythm [78]. Bursts of prefrontal theta may or may not be coherent with the hippocampal theta rhythm (fig. 9), indicating that the hippocampal signal may indeed be indispensable for the present analysis. Thus prefrontal theta phase-locking represents an aspect of cortical neuronal activity that can only be quantified and studied by direct comparison with simultaneous electrophysiological activity in the hippocampus.

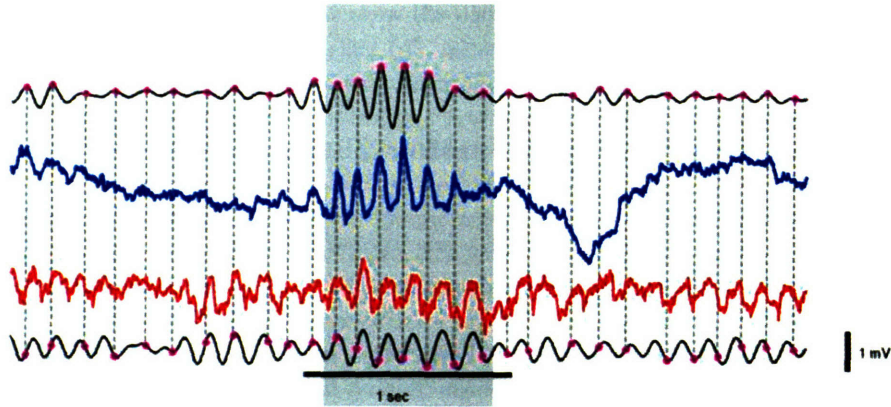


Figure 9: **Example of intermittent theta in a prefrontal LFP:** Prefrontal (blue) and hippocampal (red) LFPs and their corresponding θ band filtered traces (black) are displayed over a timespan of 4 seconds. Note the burst of prefrontal theta in a period lasting less than a second, marked by the gray patch. The peaks of the prefrontal θ -filtered trace (top) are identified and marked by the dashed vertical lines. Note that they do not align with the peaks, or any other phase, of the hippocampal theta (bottom), demonstrating the absence of coherence.

3.2 Phase-locking as an independent dimension of neuronal activity

In section 2.4 we explicitly showed that phase-locking depends on the entrainment of neuronal activity to the frequency fluctuations of the ongoing hippocampal theta oscillations. What is not immediately apparent is that phase-locking is possible in the absence of rhythmicity of neuronal firing and, conversely, rhythmicity of neuronal firing in the theta band can exist without phase-locking. We illustrate these points with two example hippocampal cells (fig. 10). In addition, neuronal firing rate, within the physiologically relevant range, imposes no constraints on phase-locking properties either. Thus phase-locking represents an independent dimension along which neuronal activity varies and can therefore be quantified and studied.

3.3 Mechanism responsible for prefrontal phase-locking

Our results show the presence of directionality in hippocampo-prefrontal interactions with hippocampal activity leading activity in prefrontal cortex on average by 50 ms (sect. 2.5, 2.6). Additionally all prefrontal cells that showed significant correlations with the hippocampal cells over a range of positive

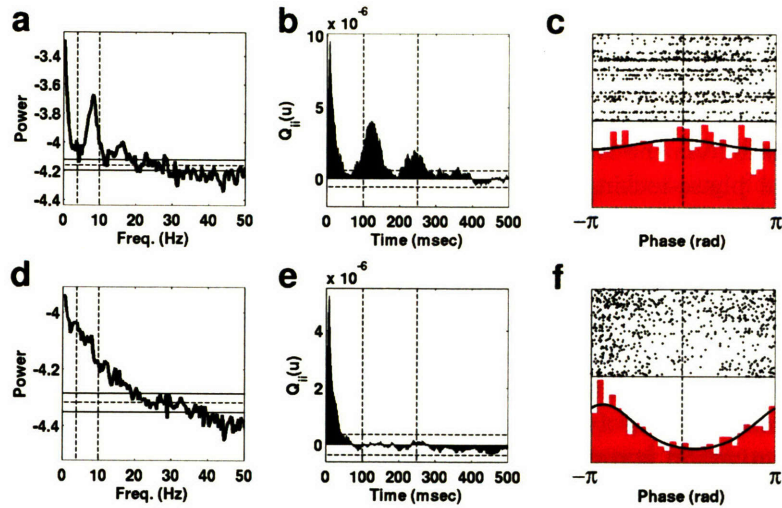


Figure 10: **Firing rhythmicity is independent of phase-locking:** Power spectral density (PSD) estimates (a,d), auto-covariances (b,e), and phase value distributions (c,f), for two hippocampal cells. The firing of the first cell (top) was rhythmic in the θ band, but it was not phase-locked to the hippocampal theta rhythm. In contrast, the firing of the second cell (bottom) was not rhythmic, but it was clearly phase-locked.

delays up to 150 ms were phase-locked (sect. 2.7). These data suggest that the direct hippocampal-PFC pathway, originating in CA1/subiculum, plays a crucial role in entraining prefrontal neuronal discharges to the hippocampal theta rhythm [28, 29, 32]. This glutamatergic pathway has a conduction velocity of approximately 0.6 m/s and corresponding mean conduction delay of 16 ms [79, 30]. In addition to the monosynaptic activation mediated via the above pathway, there is evidence for polysynaptic activation of prefrontal pyramidal neurons in response to CA1 stimulation with corresponding latency of 40 ms [80]. The broad range of delays over which significant hippocampo-prefrontal single cell correlations were observed indicates that both monosynaptic and polysynaptic activation contributed to the entrainment of prefrontal cells to the hippocampal theta rhythm.

Recent evidence has demonstrated that CA1/subiculum neurons form monosynaptic excitatory connections not only with prefrontal pyramidal cells, but also with several classes of interneurons in mPFC [81]. This feed-forward inhibition has a latency slightly smaller than the one of the monosynaptic hippocampo-prefrontal excitatory input [81]. This fact sug-

gest the intriguing possibility that phase-locking in mPFC might arise at least in part not through theta modulated excitatory drive to pyramidal cells, but also through the modulation of prefrontal pyramidal cell excitability, mediated via the local inhibitory network. This could also help explain prefrontal phase-locking even in the apparent absence of θ power in prefrontal LFPs. If a major portion of the theta modulated output from the hippocampus terminates on prefrontal interneurons rather than on pyramidal cells, the rhythmic synaptic currents it generates are unlikely to add up to a macroscopic field oscillation, because of the random geometric arrangement of interneuronal dendrites and their relatively small size. In turn, the rhythmic inhibitory output of the interneurons will tend to generate synaptic currents of relatively small amplitudes and variable polarity, dependent on the activation state of the pyramidal cells, since the reversal potential of the relevant GABA_A conductance is close to the membrane resting potential. Thus rather than hyperpolarizing pyramidal cells, the hippocampo-prefrontal feed-forward inhibition can act to rhythmically decrease pyramidal cell input impedance, thus theta-modulating their excitability.

Our evidence for direct hippocampal involvement in prefrontal phase-locking is only correlative and identifying the precise circuit mechanisms that are responsible for the theta modulation of prefrontal firing is an important open problem raised by the results presented here. There are several mechanisms that could be responsible for the observed phenomena, beyond the possibility of direct rhythmic hippocampal input to prefrontal circuits. In particular, both hippocampal and cortical cells could be co-modulated at θ frequency from sub-cortical structures, or both co-modulation and direct hippocampal rhythmic input could be contributing to the observed effect. Furthermore, resonant properties of individual cells may modulate theta phase-locking properties [82, 83, 84, 85, 86, 87]. These resonant properties may be controlled through external levels of neurotransmitters and phase-locking may thus be due to a combination of a permissive/modulating action and pacemaker rhythmic interactions.

3.4 Functional significance of prefrontal phase-locking

The demonstrated phase-locking of prefrontal neurons to the hippocampal theta rhythm is a form of neuronal *timing relationship*. Therefore it has implications for theories that posit that the timing of neuronal discharges is important for function. The list of such theories is too long and will not be reviewed here. Instead we briefly speculate on the roles phase-locking might play over short and long timescales and relate these to the two main

functions involving hippocampal and prefrontal circuits: working and long term memory.

Over short time scales, i.e. in the order of several theta cycles, phase-locking can introduce consistent temporal ordering of the excitability windows of phase-locked neurons that can be utilized for directing flow and maintaining activity in neuronal networks. Given two reciprocally connected neurons whose excitability is modulated by the same oscillatory rhythm, but with a given phase offset, the sensitivity of each neuron to the outputs of the other will be differentially affected. Thus the neuron whose excitability window precedes that of the other will be more likely to drive its target effectively. Reversing the phase offset of the modulatory rhythm will reverse the effective direction of activity flow. Elaborating on this simple model one can see how a rhythmic modulatory influence acting on several interconnected brain regions via variable delays can gate inputs and outputs and determine the direction of activity flow. Furthermore, if several such regions are interconnected so that the sum of transmission and activation delays over a return path is in the order of 150 ms, theta phase-locking can stimulate the emergence of resonant phase-locked loops [88], that can be utilized to maintain a pattern of persistent activity, a hypothesized neural correlate of short-term memory [89, 90]. Our results demonstrate that the hippocampus can play an important role in the entrainment of excitability in prefrontal cortex and therefore may represent an active element of the brain's gating and synchronizing circuitry.

Over longer time scales, phase-locking can introduce consistency in the relative timing of firing within subsets of co-activated prefrontal and hippocampal cells. Because of the properties of spike timing dependent plasticity (STDP) [91, 92], such consistency would produce a tendency toward the selective strengthening of synapses from cells with earlier preferred phases to cells with later preferred phases, as well as toward the weakening of synapses between cells with the opposite phase relation. This would stimulate the natural formation of resonant loops across cortico-hippocampal networks [88]. Loop membership would be uniquely determined by the pattern of neuronal co-activation, driven by the external input and hence uniquely representing the experience of the animal. Thus, phase-locking may be important for the formation of long-term memories and quantifying the dynamics of phase-locking properties associated with learning may be a way of identifying functionally important cortical neuronal assemblies, which may not be accessible by analyzing firing rate profiles alone.

4 Methods

4.1 Behavioral tasks

Recordings were obtained while rats performed a variety of spatial tasks in familiar environments. The tasks were 20 to 90 minutes long and included spatial working memory on an 8-arm maze, a delayed alternation on a T-maze, and exploration of linear and circular tracks.

4.2 Electrophysiological recordings

Electrophysiological signals were obtained using the technique of tetrode recordings [93]. Each tetrode consisted of four tightly bound micro-wires (each $\approx 12 \mu\text{m}$ in diameter) connected to four independent recording channels that together allowed the isolation of the activity of up to 20 single neurons in the hippocampus and up to 10 neurons in the neocortex through a process analogous to triangulation (figs. 12, 13). Four male Long-Evans 3-7 month old rats were surgically implanted with custom-built multi-site micro-drive arrays that allow targeting of multiple brain regions and independent adjustment of 18 individual tetrodes (fig. 11). The coordinates of the simultaneously targeted brain structures were (bregma, lateral) in mm: (1) medial prefrontal cortex: two groups of tetrodes centered at (+4.2,+0.5), (+2.6,+0.5); (2) hippocampus: two groups of tetrodes centered at (-3.6,+2.2), (-6.0,+5.4) targeting the CA1 subfield. Individual tetrodes were lowered to their targets in very small increments over the course of several days and further adjusted in order to maximize unit yield, isolation, and stability (fig. 13). The signal from each channel of each tetrode was first buffered at a head-stage preamplifier, analog filtered, and differentially amplified (300 Hz to 9 KHz for unit recordings, 0.1 Hz to 475 Hz for LFP recordings). Signals were referenced against area-specific dedicated electrodes positioned to minimize local unit activity. The amplifier outputs were sampled at 31.25 KHz (unit) or 1.5 KHz (LFP) and stored to disk for off-line analysis.

4.3 Signal source separation

As outlined in figure 12 the spiking activity of multiple neurons was recorded on each of the 4 tetrode channels. The first step in the data analysis was therefore to separate all recorded spikes into groups based on the source neurons that generated them. This represents an inverse transformation that is

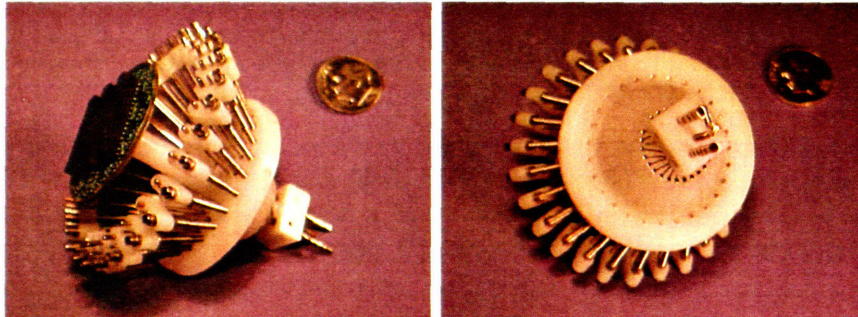


Figure 11: **Modular precision machined microdrive array:** An 18 tetrode modular array that we designed and machined is shown above. The side view (left) reveals the IC electrode interface board used to connect the tetrodes to the data acquisition hardware.

generally ill-posed, since no *a priori* information is available about the structure of the medium from which the recordings are derived. Some assumptions were thus necessary in order to constrain the problem. We assumed that the recording medium was relatively homogeneous as far as conductivity is concerned and that the bulk of the current responsible for the initial action potential generation was spatially localized. Given these assumptions a spike generated in a given location in space relative to the tetrode tip will map to a unique set of amplitudes on the 4 recording channels. Letting each spike be represented by a point in 4 dimensional *amplitude space* with coordinates given by the spike amplitudes on each of the 4 recording channels (fig. 13), it then follows that tight clusters of points in amplitude space correspond to spikes that must have been generated at roughly the same spatial location in the recording medium and thus likely belonged to the same neuron. The signal source separation procedure involved the following steps. First, all recorded spikes were converted into points in amplitude space. Then the point density was estimated over the amplitude space and the regions of elevated point density completely surrounded by regions of low point density were classified as single units. Similarly, the regions of elevated point density that were not completely surrounded by regions of low point density were classified as multi-units. Finally, the region in amplitude space close to the noise threshold was classified as unresolved background activity. At the end of the signal source separation procedure the activity of each putative single unit was succinctly represented by its corresponding set of spike times. Single units were counted for each behavioral epoch. A

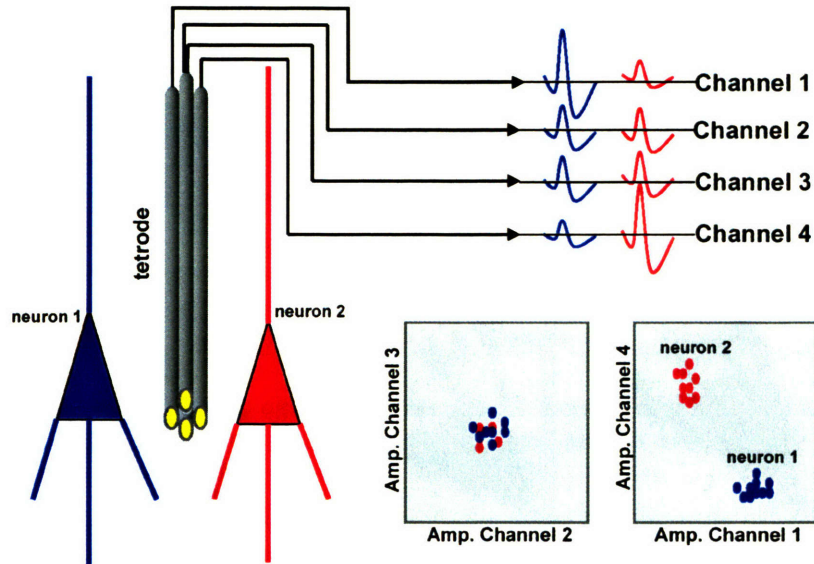


Figure 12: **Principle of tetrode recordings:** A schematic of a tetrode and two cells (colored blue and red) are shown above. Because of the spatial separation between the four tips of the tetrode and the signal sources, electrophysiological signals are differentially attenuated at each of the four tips. For example, an action potential generated by the blue cell will be picked up with high amplitude on channel 1, low on channel 4, and intermediate on channels 2,3. Conversely, an action potential generated by the red cell will have a high amplitude on channel 4, small on channel 1, and intermediate on channels 2,3. Hence it would not be possible to disambiguate the signal sources by comparing the amplitudes on channels 2,3. However, if we plot the spike amplitude on channel 1 vs. the amplitude on channel 4, spikes from the blue and red cell fall into two clearly separable clusters of points.

conservative estimate of the unique single units was obtained by counting units recorded from the same tetrode over different behavioral epochs or days only once, i.e. on one given day and epoch.

4.4 Phase-locking analysis outline

The objective of the phase-locking analysis was to study the timing relationship between a continuously varying signal (a given frequency band of the LFP) and a point process (a given spike train). While classic linear time-invariant (LTI) systems analysis has been extended to handle such hybrid data [94] it was of limited use to us because its measures combine both

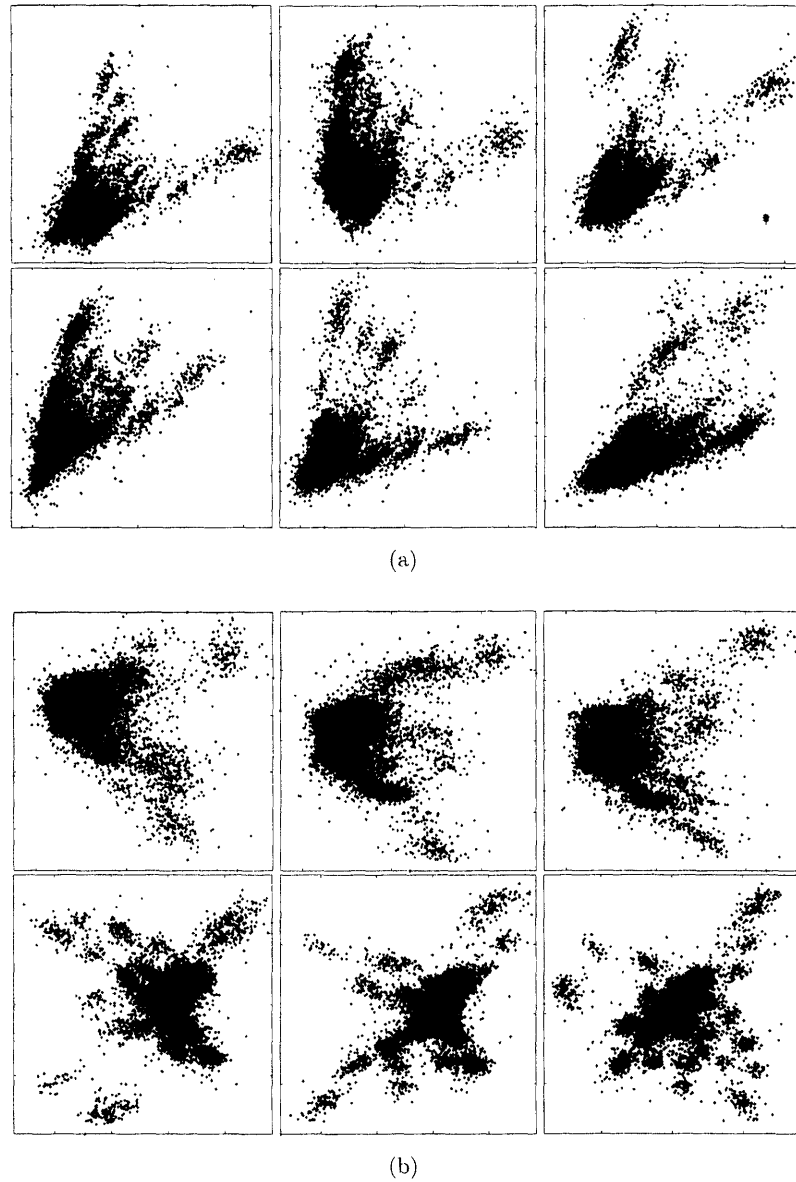


Figure 13: **Raw tetraode recordings from the pyramidal cell layer in the CA1 region of the hippocampus:** (a) Each panel is a scatter plot of spike amplitudes as seen on all pairs of the 4 tetraode channels. A linear transformation (rotation) of the data in (a) is shown in (b), rendering the multiple cleanly isolatable clusters more visible.

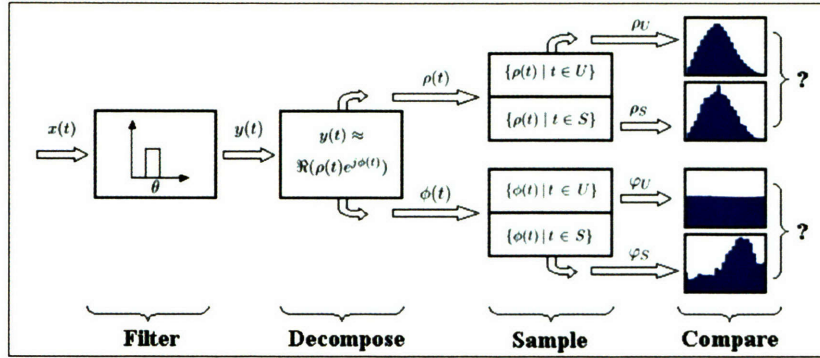


Figure 14: **Phase-locking analysis outline:** The 4 steps involved in the phase-locking analysis are depicted above. See section 4.4 for detailed description.

amplitude and phase variation and thus do not allow for the study of each in isolation. Our approach to detecting phase-locking consisted of four steps. First, the LFP signal was bandpass filtered isolating the band of interest in the resulting trace. Second, the filtered LFP was decomposed as the real part of the product of a non-negative amplitude function $\rho(t)$ and a complex exponential with time varying instantaneous phase $e^{j\phi(t)}$. Third, $\rho(t)$ and $\phi(t)$ were both sampled at dense regularly spaced points in time $t \in U = \{k \Delta t | k \in \{1, 2, \dots, T\}\}$ yielding the underlying amplitude and phase value distributions of the LFP ρ_U and φ_U , as well as at a given unit's spike times $t \in S = \{\tau_k | k \in \{1, 2, \dots, E\}\}$ yielding the unit's distributions ρ_S and φ_S . Fourth, ρ_S was compared against ρ_U and φ_S against φ_U . Intuitively if there is no relation between the filtered LFP signal and a given spike train, the unit's sampling process will be random and the sampled distributions will replicate the underlying ones. Alternatively, if a neuron fires preferentially around a given phase of the filtered LFP, the sampling will be non-random and the resulting sampled phase-value distribution will be different from the underlying one.

4.5 LFP filtering

Hippocampal LFP traces were bandpass filtered in the θ band (4-10 Hz) using digital filters constructed via the Parks-McClellan optimal equiripple FIR filter design [95]. Transition bands were 4 Hz to 4.5 Hz and 10 Hz to 10.5 Hz. Maximal ripple in the stop bands was 0.05 and 0.01 in the pass band. In order to faithfully preserve the theta wave shape in the filtered trace a wider bandpass filter was also employed in conjunction with the

subset of decomposition methods utilizing zero crossings outlined below. In this case the transition bands were 4 Hz to 4.5 Hz and 40 to 40.5 Hz with 0.01 maximal ripple in the stop and pass bands. The LFP signal used to extract the theta rhythm was always derived from the same tetrode in each animal and was selected on the basis of the robustness of the θ component. The narrow distribution of hippocampal preferred phases shown in figure 5(a) indicates a relative consistency in the phase relationships of the θ reference LFP signals used in the analysis of data from different animals.

4.6 Instantaneous amplitude/phase decomposition

Seven alternative methods were used to decompose the filtered LFP $y(t)$ into instantaneous amplitude $\rho(t)$ and phase $\phi(t)$ components such that $y(t) \approx \text{Re}(\rho(t)e^{j\phi(t)})$. In all but one methods the instantaneous amplitude and phase were defined for a subset of special points in time and the rest of the values were obtained by linear interpolation. In the *minima* method the special points were the troughs of $y(t)$ identified as the negative to positive zero crossings of the derivative $\frac{dy}{dt}$ and they were assigned instantaneous phase of $-\pi$ radians. In the *maxima* method the special points were the peaks identified as the positive to negative zero crossings of $\frac{dy}{dt}$ and were assigned instantaneous phase of 0 radians. In the *extrema* method both peaks and troughs were identified and assigned corresponding phase values as above. Analogously in the *up* and *down* methods the special points were the negative to positive and positive to negative zero crossings of $y(t)$ and they were assigned instantaneous phases of $-\frac{\pi}{2}$ and $\frac{\pi}{2}$ radians respectively. In the *zero crossing* method both types of zero crossings were identified and assigned corresponding phase values. The instantaneous amplitude at extrema was set to $|y(t)|$ while at zero crossings it was set to a value that equated the power of $y(t)$ and the approximating signal over the half cycle centered at the zero crossing. Finally in the *analytic signal* method the Hilbert transform $y_H(t)$ of $y(t)$ was computed and the analytic signal $z(t) = y(t) + jy_H(t) = \rho(t)e^{j\phi(t)}$ provided instantaneous amplitude and phase values everywhere.

The methods above have different combinations of advantages and drawbacks. The major advantage of the analytic signal decomposition is that it is exact in the sense that $y(t) = \text{Re}(\rho(t)e^{j\phi(t)})$ for all t and has differentiable instantaneous phase and angular frequency. Yet the phase values at extrema and zeros are not guaranteed to be what one would expect (i.e. $-\pi$, 0, and $\pm\frac{\pi}{2}$) and the angular frequency can take on negative values. Furthermore, since the decomposition is exact even when the input contains a

mixture of signal and noise, both enter the instantaneous phase and amplitude components and thus any denoising must occur at the earlier filtering step. This dictates the use of narrow band filters in conjunction with this method that can distort the input signal waveform. The remaining methods can be seen as fitting parametric models of reduced complexity to the input signal. The representations are exact only at their corresponding subsets of special points and both phase and amplitude components are piecewise linear, thus sacrificing differentiability and continuity at special points of the instantaneous phase and angular frequency respectively. The susceptibility of this class of methods to noise depends on the reliability with which special points can be identified, which in turn depends on the shape of the input signal. Therefore they offer robust estimates of instantaneous phase and amplitude only in combination. Finally, the uniformity of the underlying phase value distribution φ_U is guaranteed only for methods that define one special point per wave cycle, i.e. *minima*, *maxima*, *up*, and *down*. The use of multiple methods for phase extraction makes subsequent analysis robust to signal deviation from model assumptions.

4.7 Effects of theta waveform asymmetry

Depending on the method employed for obtaining the instantaneous phase, $\phi(t)$, subtle complications can arise in the presence of θ waveform asymmetry. To see why this is the case, consider a fictitious sawtooth θ waveform with peak-to-trough time longer than trough-to-peak time, and a cell whose spikes are randomly distributed in time. Because of the asymmetry of the above waveform, more of the spikes will occur during the falling half of the θ cycle, leading to a non-uniform phase value distribution and an incorrect quantification of the phase-locking properties of the cell.

The above problem is not merely of theoretical interest, as the experimentally observed θ waves indeed have an asymmetric sawtooth shape [96, 5]. The presence and form of the asymmetry depend on the precise position of the electrode, the behavior of the animal, and the method used to extract the instantaneous phase function $\phi(t)$ from the θ -filtered LFP trace. The consequences of the asymmetry for phase-locking analysis can be explicitly evaluated by examining the underlying distribution of phase values φ_U obtained through uniform sampling of $\phi(t)$ (fig. 15, see below). Deviations from uniformity in φ_U as small as 2% can produce false positive phase-locking detection in excess of 10% at $p=0.01$ for an untuned unit with mean firing rate of 5 Hz recorded over a period of an hour. The false positive rate grows with the number of recorded spikes, which can be high not

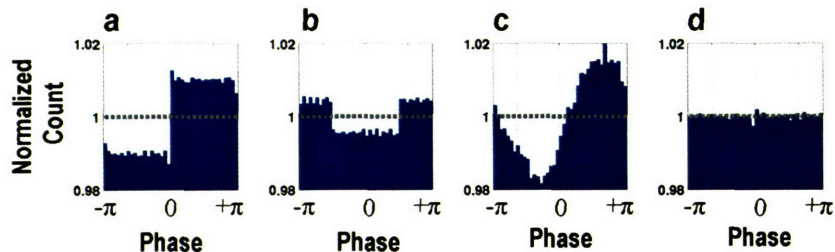


Figure 15: **Theta phase value distributions of a hippocampal LFP under different phase extraction methods:** (a-d) Phase value distributions φ_U corresponding to a 37 minute θ -filtered hippocampal LFP trace extracted by extrema, zero crossing, hilbert, and maxima methods. Only methods that define a single special point per wave cycle are expected to yield uniform φ_U as in (d). The precise distribution of φ_U for the other methods will depend on the waveshape and its symmetry and can clearly be non-uniform as in (a-c). Although in these cases the maximum deviation from uniform density (gray lines) is less than 2 %, a random sample of φ_U generated at a mean rate of 10 Hz has about 15 %, instead of 1 %, chance of being erroneously detected as phase-locked at $\alpha = 0.01$ significance level. Similarly a weakly phase-locked unit with preferred phase around the minimum of φ_U is likely to be misclassified as unlocked.

only because of a high mean firing rate, but also because of a long recording duration. Ultimately, if a sufficiently large number of spikes are recorded, the error will approach 100%.

4.8 Phase value distributions φ_U and φ_S

The amplitude/phase decomposition yields phase values $\phi(t)$ at the sample times $U = \{t = k\Delta t | k \in \{1, 2, \dots, T\}\}$, where $\Delta t \approx 0.67$ (ms) is the sampling period and $T\Delta t$ is the duration of the recording. The underlying phase value distribution is defined as $\varphi_U = \{\phi(t) | t \in U\}$. If a unit has generated N spikes at times $S = \{\tau_k | k \in \{1, 2, \dots, N\}\}$ its phase value distribution is given by $\varphi_S = \{\phi(t) | t \in S\}$. Thus φ_S can be regarded as a sample drawn from φ_U .

4.9 Comparing φ_S and φ_U

If S is a random sample of U then φ_S will replicate the distribution of φ_U . In particular, if φ_U is uniform then under random sampling so would φ_S .

Uniformity of φ_U is particularly desirable because in this case the question of phase-locking detection, i.e. whether or not φ_S is a random sample of φ_U , reduces to simply detecting departures from uniformity in φ_S , which is readily done by the tools of circular statistics.

Fortunately we can devise a transformation $\Psi : [-\pi, \pi) \rightarrow [-\pi, \pi)$ such that $\varphi_U^\Psi = \Psi(\varphi_U) = \{\Psi(x) | x \in \varphi_U\}$ is uniform. If we similarly let $\varphi_S^\Psi = \Psi(\varphi_S) = \{\Psi(x) | x \in \varphi_S\}$ be the Ψ -transformed unit phase value distribution then testing for the presence of phase-locking amounts to testing whether φ_S^Ψ is uniform. To ease notation we use φ_S to refer to the Ψ -transformed unit phase value distribution.

Let $F_U : [-\pi, \pi) \rightarrow [0, 1)$ be the empirical cumulative distribution function (cdf) corresponding to φ_U . Then $\Psi(x) = 2\pi F_U(x) - \pi$ yields the desired transformation. The transformation Ψ is equivalent to the computation of the *circular ranks* or *uniform scores* of the elements of φ_U . Clearly if φ_U is uniform to begin with Ψ reduces to the identity map.

4.10 Phase-locking detection and characterization

The presence of phase-locking was evaluated by applying the Rayleigh test for circular uniformity on the Ψ -transformed unit phase value distribution φ_S . Briefly, given n phase values ϕ_i define the first *trigonometric moment* $m' = \frac{1}{n} \sum_{i=1}^n e^{j\phi_i} = \bar{R}e^{j\mu}$. The sample mean direction or preferred phase μ is given by the orientation of m' , while the mean resultant length \bar{R} by the modulus of m' . The Rayleigh statistic is $Z = n\bar{R}^2$ and the probability that the null hypothesis of sample uniformity holds is given by $P = e^{-Z} [1 + (2Z - Z^2)/(4n) - (24Z - 132Z^2 + 76Z^3 - 9Z^4)/(288n^2)]$. For $n > 50$ the approximation $P = e^{-Z}$ is adequate [97, 98, 99].

The Rayleigh test evaluates the hypothesis of uniformity against a *unimodal* alternative. Thus if φ_S is bimodal with opposite modes the Rayleigh test will likely fail to reject the null hypothesis. There of course exist procedures for testing uniformity against *any* alternative. In particular Kuiper's test is an extension of the Kolmogorov-Smirnov test for circular data that can be successfully applied in cases involving multi modal phase value distributions. However in our definition phase-locking represented a unimodal alternative to uniform phase value distribution and thus the Rayleigh test was the most appropriate.

All significantly phase-locked units were fit with a von Mises distribution with density $f(\phi) = \frac{1}{2\pi I_0(\kappa)} e^{\kappa \cos(\phi - \mu)}$, for $-\pi \leq \phi < \pi$ and $0 \leq \kappa < \infty$ [97, 98, 99]. The maximum likelihood (ML) estimate for the von Mises mean direction parameter is equal to the sample mean direction μ . The ML

estimate for the concentration parameter κ is given by the solution of the equation $\frac{I_1(\kappa)}{I_0(\kappa)} = \bar{R}$, where $I_i(x)$ is the modified Bessel function of order i . The solution was obtained by using a numerical zero finding routine.

4.11 Cross-covariance analysis

In order to quantify the interactions between pairs of simultaneously recorded spike trains, we considered each pair to be the realization of a stationary bivariate stochastic point process (N_i, N_j) , where $N_i(t)$ indicates the number of spikes generated by neuron i in the time interval from 0 to t [100, 101]. The differential increment at time t is defined as $dN(t) = (N(t+dt) - N(t))$ and counts the number of events in the small interval $(t, t+dt]$. For an orderly point process, $dN(t)$ takes the values of zero or one depending on whether or not a spike has occurred in the time interval between t and $t+dt$. The *mean intensity* P_i of the point process N_i is defined as $E\{dN_i(t)\} = P_i dt$ and corresponds to the mean firing rate in the units of the time axis. The *cross-product density* at lag u , $P_{ij}(u)$, between the point processes N_i and N_j is defined as $E\{dN_i(t+u)dN_j(t)\} = P_{ij}(u) du dt$ and can be interpreted as the probability of co-occurrence of a N_i event in the interval $(t+u, t+u+du]$ and a N_j event in $(t, t+dt]$ [102, 103]. Finally the *cross-covariance* function, $q_{ij}(u)$, defined as $cov\{dN_i(t+u), dN_j(t)\} = q_{ij} du dt$ can be expressed as $q_{ij}(u) = P_{ij}(u) - P_i P_j$. If the two spike trains are independent, $P_{ij}(u) = P_i P_j$ and consequently $q_{ij}(u) = 0$. Therefore the null hypothesis, H_0 , of no interaction between N_i and N_j can be rejected if an estimate $\hat{q}_{ij}(u)$ of the cross-covariance function deviates significantly from 0.

We estimated the cross-covariance function between spike trains N_i and N_j in the time domain on the basis of the *cross-correlation histogram* $J_{ij}^{T,b}(u)$, which counts the number of spike pairs occurring at times (τ_{im}, τ_{jn}) , such that $|\tau_{im} - \tau_{jn} - u| < b/2$, with b specifying the bin size and T the period of observation. We used the cross-covariance estimate $\hat{q}_{ij}(u) = J_{ij}^{T,b}(u)/(bT) - \hat{P}_i \hat{P}_j$, where $\hat{P}_i = N_i(T)/T$ and $\hat{P}_j = N_j(T)/T$ [102, 103]. The asymptotic distribution of $\hat{q}_{ij}(u)$ is approximately normal $N\{\mu = q_{ij}(u), \sigma^2 = P_{ij}(u)/(bT)\}$ [103] and consequently under the null hypothesis H_0 of spike train independence $\hat{q}_{ij}(u) \sim N\{\mu = 0, \sigma^2 = P_i P_j/(bT)\}$. Since the variance of $\hat{q}_{ij}(u)$ under H_0 depends on the mean firing rates, bin size, and period of observation, we used a standardized cross-covariance, $Q_{ij}(u) = \sqrt{\frac{bT}{\hat{P}_i \hat{P}_j}} \hat{q}_{ij}(u)$, so that $Q_{ij}(u) \sim N\{\mu = 0, \sigma^2 = 1\}$ under H_0 . Therefore H_0 could be rejected when $|Q_{ij}(u)| > Z_{\alpha(2)}$ for some u , where $Z_{\alpha(2)} =$

$\sqrt{2} \operatorname{erf}^{-1}(1 - \alpha)$ is the two-tailed critical z-value at level α . Standardizing the cross-covariance estimates allowed us to meaningfully compare, combine, and display $Q_{ij}(u)$ on a common scale.

We computed $Q_{ij}(u)$ for all 3617 pairs of simultaneously recorded prefrontal and hippocampal units, over time lags u between ± 512 ms in 1 ms steps using a 15 ms bin. Thus for each pair of spike trains, $Q_{ij}(u)$ was a sequence of 1025 values. Since H_0 could be rejected at each lag we lowered our target $\alpha = 0.01$ by 1025 giving a lag-corrected critical z-value of 4.42. Under these conditions 948 or 26 % of the pairs were deemed to have significant interactions. However this treatment is only asymptotically correct and for spike trains with small numbers of events can produce spurious significant correlations. To see why this is the case note that under the null hypothesis $J_{ij}^{T,b}(u) \sim \text{Poisson}\{\lambda = bT P_i P_j\}$ [102] and $Q_{ij}(u)$ can be expressed as $Q_{ij}(u) = (J_{ij}^{T,b}(u) - \hat{\lambda})/\sqrt{\hat{\lambda}}$, where $\hat{\lambda} = bT \hat{P}_i \hat{P}_j$. Thus $Q_{ij}(u)$ can be viewed as a standardized cross correlation histogram and $Q_{ij}(u)$ is approximately normal when the normal approximation to the Poisson distribution applies, i.e. for $\lambda > 20$, which gives the condition $bT \hat{P}_i \hat{P}_j > 20$. Given a recording duration T of 30 minutes and bin size b of 15 ms, the product of the firing rates in Hz must exceed 0.75 in order for the approximation to apply. Since about half of the recorded units had mean firing rates under 0.75 Hz spurious significant cross covariance functions were seen, displaying characteristic narrow peaks and troughs (width in the order of b , i.e. 15 ms). Spurious $Q_{ij}(u)$ could be eliminated by restricting the cross-covariance analysis only to the 708 spike train pairs with sufficiently high mean firing rates. Under these conditions 134 or 19 % of the qualifying pairs had significant interactions. However this restriction disqualified almost 51 % of the prefrontal units from entering the analysis. Therefore instead of biasing the analysis by imposing minimal firing rate restrictions, we accepted possibly spurious $Q_{ij}(u)$, with the understanding that they could only contribute unstructured noise that would be attenuated in subsequent averaging. This was explicitly verified by repeating the analysis with the minimal firing rate restriction imposed.

The standardized mean cross covariance, $Q_i(u)$, between prefrontal unit i and the simultaneously recorded population of hippocampal units was computed as $Q_i(u) = \frac{1}{\sqrt{K}} \sum_{j=1}^K Q_{ij}(u)$ where the index j ran over the K hippocampal units exhibiting significant interactions with i . The $\frac{1}{\sqrt{K}}$ factor was applied so that $Q_i(u)$ was approximately normal $N\{\mu = 0, \sigma^2 = 1\}$ under the null hypothesis of independence between N_i and *all* N_j . The mean squared cross-covariance, $Q_i^s(u)$, was computed as $Q_i^s(u) = \frac{1}{K} \sum_{j=1}^K Q_{ij}^s(u)$.

This measure controlled for the possible cancellation of significant, but opposite covariance structure allowed by $Q_i(u)$. When $Q_i(u)$ or $Q_i^g(u)$ were averaged over a subset L of prefrontal units the resulting quantities were denoted as $\langle Q_i(u) \rangle_L = \frac{1}{|L|} \sum_{i \in L} Q_i(u)$, with an analogous expression for $\langle Q_i^g(u) \rangle_L$.

We also repeated the entire analysis based on cross-covariance estimates constructed in the frequency domain as the inverse Fourier transform of the cross-spectrum, computed using the method of disjoint sections [94]. All results we report here were qualitatively unaffected by the estimation procedure.

References

- [1] Squire L.R. Memory and the hippocampus: A synthesis from findings with rats, monkeys, and humans. *Psychological Review*, 99(2):195–231, 1992.
- [2] Fuster J.M. *The Prefrontal Cortex: Anatomy, Physiology, and Neuropsychology of the Frontal Lobe*. Lippincott-Raven, 3rd edition, 1997.
- [3] Green J.D. and Arduini A.A. Hippocampal electrical activity in arousal. *J. Neurophysiol.*, 17:533–557, 1954.
- [4] Vanderwolf C.H. Hippocampal electrical activity and voluntary movement in the rat. *Electroencephalogr. Clin. Neurophys.*, 26:407–418, 1969.
- [5] Buzsáki G. Theta oscillations in the hippocampus. *Neuron*, 33:325–340, 2002.
- [6] Scoville W.B. and Milner B. Loss of recent memory after bilateral hippocampal lesions. *J. Neurol. Neurosurg. Psychiatry*, 20:11–21, 1957.
- [7] Milner B., Corkin S., and Teuber H.-L. Further analysis of the hippocampal amnesic syndrome: 14-year follow-up study of H.M. *Neuropsychologia*, 6:215–234, 1968.
- [8] Squire L.R., Clark R.E., and Knowlton B.J. Retrograde amnesia. *Hippocampus*, 11(1):50–55, 2001.
- [9] Corkin S. What’s new with the amnesic patient H.M.? *Nat. Rev. Neurosci.*, 3:153–160, 2002.
- [10] Milner B. and Penfield W. Memory deficit produced by bilateral lesions in the hippocampal zone. *AMA Arch. Neurol. Psychiatry*, 79:475–497, 1958.
- [11] Squire L.R. Mechanisms of memory. *Science*, 232(4758):1612–9, 1986.
- [12] Squire L.R. and Zola S.M. Structure and function of declarative and non-declarative memory systems. *Proc. Natl. Acad. Sci.*, 93(24):13515–22, 1996.
- [13] Squire L.R. and Zola-Morgan S. The medial temporal lobe memory system. *Science*, 253:1380–6, 1991.
- [14] Marr D. Simple memory: a theory for archicortex. *Philos Trans R Soc Lond B Biol Sci.*, 262(841):23–81, 1971.
- [15] Rosenbaum R.S., Winocur G., and Moscovitch M. New views on old memories: re-evaluating the role of the hippocampal complex. *Behav Brain Res.*, 127(1-2):183–197, 2001.
- [16] Fries P., Fernandez G., and Jensen O. When neurons form memories. *Trends Neurosci.*, 26(3):123–4, 2003.
- [17] Lashley K.S. *Brain Mechanisms and Intelligence: a Quantitative Study of Injuries to the Brain*. Dover Publications, 1929.
- [18] Hebb D.O. *The Organization of Behavior*. Wiley, 1949.

-
- [19] Qin Y.L., McNaughton B.L., Skaggs W.E., and Barnes C.A. Memory reprocessing in corticocortical and hippocampocortical neuronal ensembles. *Philos Trans R Soc Lond B Biol Sci.*, 352(1360):1525–33, 1997.
- [20] Hoffman K.L. and McNaughton B.L. Coordinated reactivation of distributed memory traces in primate neocortex. *Science*, 297(5589):2070–3, 2002.
- [21] Sutherland G.R. and McNaughton B. Memory trace reactivation in hippocampal and neocortical neuronal ensembles. *Curr Opin Neurobiol.*, 10(2):180–6, 2000.
- [22] M.A. Wilson and B.L. McNaughton. Reactivation of hippocampal ensemble memories during sleep. *Science*, 265:676–679, 1994.
- [23] Louie K. and Wilson M.A. Temporally structured replay of awake hippocampal ensemble activity during rapid eye movement sleep. *Neuron*, 29:145–156, 2001.
- [24] Lee A.K. and Wilson M.A. Memory of sequential experience in the hippocampus during slow wave sleep. *Neuron*, 36(6):1183–94, 2002.
- [25] Siapas A.G. and Wilson M.A. Coordinated interactions between hippocampal ripples and cortical spindles during slow-wave sleep. *Neuron*, 21:1123–1128, 1998.
- [26] Sirota A., Csicsvari J., Buhl D., and Buzsáki G. Communication between neocortex and hippocampus during sleep in rodents. *Proc. Natl. Acad. Sci.*, 100(4):2065–9, 2003.
- [27] Buzsáki G. Two-stage model of memory trace formation: a role for "noisy" brain states. *Neuroscience*, 31(3):551–70, 1989.
- [28] Swanson L.W. A direct projection from ammon's horn to prefrontal cortex in the rat. *Brain Res.*, 217:150–154, 1981.
- [29] Jay T.M., Glowinski J., and Thierry A.M. Selectivity of the hippocampal projection to the prelimbic area of the prefrontal cortex in the rat. *Brain Res.*, 505:337–340, 1989.
- [30] Jay T.M., Thierry A.M., Wiklund L., and Glowinski J. Excitatory amino acid pathway from the hippocampus to the prefrontal cortex. contribution of AMPA receptors in hippocampo-prefrontal cortex transmission. *Eur. J. Neurosci.*, 4:1285–1295, 1992.
- [31] Cavada C., Llamas A., and Reinoso-Suarez F. Allocortical afferent connections of the prefrontal cortex in the cat. *Brain Res.*, 260:117–120, 1983.
- [32] Jay T.M. and Witter M.P. Distribution of hippocampal CA1 and subicular efferents in the prefrontal cortex of the rat studied by means of anterograde transport of phaseolus vulgaris-leucoagglutinin. *J. Comp. Neurol.*, 313:574–586, 1991.

-
- [33] Thierry A.M., Gioanni Y., and Dégénétais E. Hippocampo-prefrontal cortex pathway: anatomical and electrophysiological characteristics. *Hippocampus*, 10:411–419, 2000.
- [34] Laroche S., Jay T.M., and Thierry A.M. Long-term potentiation in the prefrontal cortex following stimulation of the hippocampal CA1 subicular region. *Neurosci. Lett.*, 114:184–190, 1990.
- [35] Jay T.M., Burette F., and Laroche S. NMDA receptor-dependent long-term potentiation in the hippocampal afferent fibre system to the prefrontal cortex in the rat. *Eur. J. Neurosci.*, 7:247–250, 1995.
- [36] Takita M., Izaki Y., Jay T.M., Kaneko H., and Suzuki S.S. Induction of stable long-term depression in vivo in the hippocampal prefrontal pathway. *Eur. J. Neurosci.*, 11:4145–4148, 1999.
- [37] Laroche S., Davis S., and Jay T.M. Plasticity at hippocampal to prefrontal cortex synapses: dual roles in working memory and consolidation. *Hippocampus*, 10:438–446, 2000.
- [38] Christoffersen G.R.J., Petersen S., and daCosta N.M. Potentiation of prelimbic field potentials during and seconds after trains of excitations in the rat hippocampo-prefrontal pathway. *Neuroscience Letters*, 341:143–146, 2003.
- [39] Floresco S.B., Seamans J.K., and Phillips A.G. Selective roles for hippocampal, prefrontal cortical, and ventral striatal circuits in radial-arm maze tasks with or without a delay. *J. Neurosci.*, 17(5):1880–1890, 1997.
- [40] Aujla H. and Beninger R.J. Hippocampal-prefrontocortical circuits: PKA inhibition in the prefrontal cortex impairs delayed nonmatching in the radial maze in rats. *Behav. Neurosci.*, 115:1204–1211, 2001.
- [41] Wiltgen B.J., Brown R.A., Talton L.E., and Silva A.J. New circuits for old memories: the role of the neocortex in consolidation. *Neuron*, 44:101–108, 2004.
- [42] Bontempi B., Laurent-Demir C., Destrade C., and Jaffard R. Time-dependent reorganization of brain circuitry underlying long-term memory storage. *Nature*, 400:671–675, 1999.
- [43] Frankland P.W., Bontempi B., Talton L.E., Kaczmarek L., and Silva A.J. The involvement of the anterior cingulate cortex in remote contextual fear memory. *Science*, 304:881–883, 2004.
- [44] Maviel T., Durkin T.P., Menzaghi F., and Bontempi B. Sites of neocortical reorganization critical for remote spatial memory. *Science*, 305:96–99, 2004.
- [45] Takehara K., Kawahara S., and Kirino Y. Time-dependent reorganization of the brain components underlying memory retention in trace eyeblink conditioning. *J. Neurosci.*, 23(30):9897–9905, 2003.

- [46] Winson J. Loss of hippocampal theta rhythm results in spatial memory deficit in the rat. *Science*, 201:160–163, 1978.
- [47] Mitchell S.J., Rawlins J.N., Steward O., and Olton D.S. Medial septal area lesions disrupt theta rhythm and cholinergic staining in medial entorhinal cortex and produce impaired radial arm maze behavior in rats. *J. Neurosci.*, 2(3):292–302, 1982.
- [48] Givens B.S. and Olton D.S. Cholinergic and gabaergic modulation of medial septal area: effect on working memory. *Behav. Neurosci.*, 104(6):849–855, 1990.
- [49] Greenstein Y.J., Pavlides C., and Winson J. Long-term potentiation in the dentate gyrus is preferentially induced at theta rhythm periodicity. *Brain Res*, 438:331–4, 1988.
- [50] Hölscher C., Anwyl R., and Rowan M.J. Stimulation on the positive phase of hippocampal theta rhythm induces long-term potentiation that can be depotentiated by stimulation on the negative phase in area CA1 *in vivo*. *J. Neurosci.*, 17(16):6470–6477, 1997.
- [51] Buno W. Jr., Garcia-Sanchez J.L., and Garcia-Austt E. Reset of hippocampal rhythmical activities by afferent stimulation. *Brain. Res. Bull.*, 3(1):21–8, 1978.
- [52] Williams J.M. and Givens B. Stimulation-induced reset of hippocampal theta in the freely performing rat. *Hippocampus*, 13(1):109–16, 2003.
- [53] Pedemonte M., Goldstein-Daruech N., and Velluti R.A. Temporal correlations between heart rate, medullary units and hippocampal theta rhythm in anesthetized, sleeping and awake guinea pigs. *Auton. Neurosci.*, 107(2):99–104, 2003.
- [54] Karashima A., Nakamura K., Watanabe M., Sato N., Nakao M., Katayama N., and Yamamoto M. Synchronization between hippocampal theta waves and pgo waves during rem sleep. *Psychiatry Clin. Neurosci.*, 55(3):189–90, 2001.
- [55] O’Keefe J. and Dostrovsky J. The hippocampus as a spatial map. preliminary evidence from unit activity in the freely-moving rat. *Brain Res.*, 34(1):171–5, 1971.
- [56] O’Keefe J. Place units in the hippocampus of the freely moving rat. *Exp Neurol.*, 51(1):78–109, 1976.
- [57] O’Keefe J. and Black A.H. Single unit and lesion experiments on the sensory inputs to the hippocampal cognitive map. *Ciba. Found. Symp.*, 58:179–98, 1977.
- [58] Wiener S.I., Paul C.A., and Eichenbaum H. Spatial and behavioral correlates of hippocampal neuronal activity. *J. Neurosci.*, 9(8):2737–63, 1989.

-
- [59] Bunsey M. and Eichenbaum H. Conservation of hippocampal memory function in rats and humans. *Nature*, 379(6562):255–7, 1996.
- [60] Wood E.R., Dudchenko P.A., and Eichenbaum H. The global record of memory in hippocampal neuronal activity. *Nature*, 397(6720):561–563, 1999.
- [61] Buzsáki G. and Eidelberg E. Phase relations of hippocampal projection cells and interneurons to theta activity in the anesthetized rat. *Brain Res.*, 266(2):334–9, 1983.
- [62] Buzsáki G., Leung L.W.S., and Vanderwolf C.H. Cellular bases of hippocampal EEG in the behaving rat. *Brain Res. Rev.*, 6:139–171, 1983.
- [63] Fox S.E., Wolfson S., and Ranck J.B. Hippocampal theta rhythm and the firing of neurons in walking and urethane anesthetized rats. *Exp. Brain Res.*, 62:495–508, 1986.
- [64] O’Keefe J. and Recce M. L. Phase relationship between hippocampal place units and the EEG theta rhythm. *Hippocampus*, 3(3):317–330, 1993.
- [65] Mehta M.R., Lee A.K., and Wilson M.A. Role of experience and oscillations in transforming a rate code into a temporal code. *Nature*, 417:741–746, 2002.
- [66] Harris K.D., Henze D.A., Hirase H., Leinekugel X., Dragoi G., Czurko A., and Buzsáki G. Spike train dynamics predicts theta-related phase precession in hippocampal pyramidal cells. *Nature*, 417:738–741, 2002.
- [67] Vinogradova O.S. and Brazhnik E.S. Theta-bursts of hippocampal and septal neurons. *Zh. Vyssh. Nerv. Deiat. Im. I. P. Pavlova.*, 27(6):1166–72, 1977.
- [68] Kocsis B. and Vertes R.P. Phase relations of rhythmic neuronal firing in the supramammillary nucleus and mammillary body to the hippocampal theta activity in urethane anesthetized rats. *Hippocampus*, 7(2):204–214, 1997.
- [69] Kocsis B. and Vertes R.P. Dorsal raphe neurons: synchronous discharge with the theta rhythm of the hippocampus in the freely behaving rat. *J. Neurophysiol.*, 68(4):1463–7, 1992.
- [70] Bassant M.H. and Poindessous-Jazat F. Ventral tegmental nucleus of gudden: a pontine hippocampal theta generator? *Hippocampus*, 11(6):809–13, 2001.
- [71] Chrobak J.J., Lorincz A., and Buzsáki G. Physiological patterns in the hippocampo-entorhinal cortex system. *Hippocampus*, 10(4):457–465, 2000.
- [72] Pare D. and Gaudreau H. Projections cells and interneurons of the lateral and basolateral amygdala: distinct firing patterns and differential relation to theta and delta rhythms in conscious cats. *J. Neurosci.*, 16(10):3334–3350, 1996.
- [73] Pedemonte M., Pena J.L., and Velluti A. Firing of inferior colliculus auditory neurons is phase-locked to the hippocampus theta rhythm during paradoxical sleep and waking. *Exp. Brain Res.*, 112:41–46, 1996.

- [74] Pedemonte M., Perez-Perera L., Pena J.L., and Velluti R.A. Sleep and wakefulness auditory processing: cortical units vs. hippocampal theta rhythm. *Sleep Research Online*, 4(2):51–57, 2001.
- [75] Gambini J.P., Velluti R.A., and Pedemonte M. Hippocampal theta rhythm synchronizes visual neurons in sleep and waking. *Brain Res.*, 926(1-2):137–41, 2002.
- [76] Natsume K., Hallworth N.E., Szgatti T.L., and Bland B.H. Hippocampal theta-related cellular activity in the superior colliculus of the urethane-anesthetized rat. *Hippocampus*, 9:500–509, 1999.
- [77] Colom L.V., Christie B.R., and Bland B.H. Cingulate cell discharge patterns related to hippocampal EEG and their modulation by muscarinic and nicotinic agents. *Brain Res.*, 460:329–338, 1988.
- [78] Kahana M.J., Sekuler R., Caplan J.B., Kirschen M., and Madsen J.R. Human theta oscillations exhibit task dependence during virtual maze navigation. *Nature*, 399:781–784, 1999.
- [79] Ferino F., Thierry A.M., and Glowinski J. Anatomical and electrophysiological evidence for a direct projection from ammon's horn to medial prefrontal cortex. *Exp. Brain Res.*, 65:421–426, 1987.
- [80] Degenetais E., Thierry A.M., Glowinski J., and Gioanni Y. Synaptic influence of hippocampus on pyramidal cells of the rat prefrontal cortex: an in vivo intracellular recording study. *Cereb Cortex.*, 13(7):782–792, 2003.
- [81] Tierney P.L., Degenetais E., Thierry A.M., Glowinski J., and Gioanni Y. Influence of the hippocampus on interneurons of the rat prefrontal cortex. *Eur. J. Neurosci.*, 20(3):514–524, 2004.
- [82] Leung L.S. and Yu H-W. Theta-frequency resonance in hippocampal CA1 neurons in vitro demonstrated by sinusoidal current injection. *J. Neurophys.*, 79:1592–1596, 1998.
- [83] Chapman C.A. and Lacaille J.C. Intrinsic theta-frequency membrane potential oscillations in hippocampal CA1 interneurons of stratum lacunosum-moleculare. *J. Neurophysiol.*, 81(3):1296–1307, 1999.
- [84] Hu H., Vernaeke K., and Strom J.F. Two forms of electrical resonance at theta frequencies generated by m-current, h-current and persistent sodium current in rat hippocampal pyramidal cells. *J. Physiol.*, 543(3):783–805, 2002.
- [85] Hutcheon B., Miura R.M., and Putil E. Subthreshold membrane resonance in neocortical neurons. *J. Neurophysiol.*, 76(2):683–697, 1996.
- [86] Strata F. Intrinsic oscillations in CA3 hippocampal pyramids: physiological relevance to theta rhythm generation. *Hippocampus*, 8:666–679, 1998.
- [87] Hutcheon B. and Yarom Y. Resonance, oscillation and the intrinsic frequency preferences of neurons. *TINS*, 23:216–222, 2000.

-
- [88] Miller R. *Cortico-Hippocampal Interplay and the Representation of Contexts in the Brain*. Springer-Verlag, 1991.
- [89] Goldman-Rakic P.S. Cellular basis of working memory. *Neuron*, 14(3):477–485, 1995.
- [90] Fuster J.M. The prefrontal cortex—an update: time is of the essence. *Neuron*, 30(2):319–333, 2001.
- [91] Markram H., Lubke J., Frotscher M., and Sakmann B. Regulation of synaptic efficacy by coincidence of postsynaptic APs and EPSPs. *Science*, 275:213–215, 1997.
- [92] Bi G. and Poo M. Synaptic modification in cultured hippocampal neurons: Dependence on spike timing, synaptic strength, and postsynaptic cell type. *J. Neurosci.*, 18:10464–10472, 1998.
- [93] Wilson M.A. and McNaughton B.L. Dynamics of the hippocampal ensemble code for space. *Science*, 261:1055–1058, 1993.
- [94] Halliday D.M., Rosenberg J.R., Amjad A.M., Breeze P., Conway B.A., and Farmer S.F. A framework for the analysis of mixed time series / point source data—theory and application to the study of physiological tremor, single motor unit discharges and electromyograms. *Progress in Biophysics and Molecular Biology*, 64(2/3):237–278, 1995.
- [95] Oppenheim A.V. and Schaffer R.W. *Discrete-Time Signal Processing*. Prentice Hall, 1989.
- [96] Buzsaki G., Rappelsberger P., and Kelenyi L. Depth profiles of hippocampal rhythmic slow activity ('theta rhythm') depend on behaviour. *Electroencephalogr Clin Neurophysiol.*, 61:77–88, 1985.
- [97] Fisher N.I. *Statistical Analysis of Circular Data*. Cambridge University Press, 1993.
- [98] Zar J.H. *Biostatistical Analysis*. Prentice Hall, 4th edition, 1998.
- [99] Mardia K.V. *Statistics of Directional Data*. Academic Press, N.Y., 1972.
- [100] Perkel D.H., Gerstein G.L., and Moore G.P. Neuronal spike trains and stochastic point processes. i. the single spike train. *Biophys J.*, 7(4):391–418, 1967.
- [101] Perkel D.H., Gerstein G.L., and Moore G.P. Neuronal spike trains and stochastic point processes. ii. simultaneous spike trains. *Biophys J.*, 7(4):419–40, 1967.
- [102] Brillinger D.R. Measuring the association of point processes: a case history. *American Mathematical Monthly*, 83:16–22, 1976.
- [103] Halliday D.M. and Rosenberg J.R. Time and frequency domain analysis of spike train and time series data. In Windhorst U. and Johansson H., editors, *Modern Techniques in Neuroscience Research*, chapter 18, pages 503–543. Springer-Verlag, 1999.